ADDIS ABABA UNIVERSITY

COLLEGE OF NATURAL AND COMPUTATIONAL SCIENCES

CENTER FOR ENVIRONMENTAL SCIENCE

A MASTER THESIS

SYNTHESIS, CHARACTERIZATION AND FABRICATION OF TPA-DERIVATIVE BASED DYE SENSITIZER USING TiO_2 NANOPARTICLES FOR DSSCs

By: Frehiwot Gashaw G/Mariam

Adviser: 1. Dr. Yedilfana Setarge (Ass. prof.)

2. Dr. Mekonnen Abebayehu (Ass. prof.)

June ,2024

Addis Ababa

ADDIS ABABA UNIVERSITY

COLLEGE OF NATURAL AND COMPUTATIONAL SCIENCES

CENTER FOR ENVIRONMENTAL SCIENCE

A Master Thesis

SYNTHESIS, CHARACTERIZATION AND FABRICATION OF TPA-DERIVATIVE BASED DYE SENSITIZER USING TiO_2 NANOPARTICLES FOR DSSCs

By: Frehiwot Gashaw G/Mariam

Advisors: 1. Dr. Yedilfana Setarge

2. Dr. Mekonnen Abebayehu

June, 2024

Addis Ababa

Addis Ababa University

College of Natural and Computational Sciences

Center for Environmental Science

This is to certify that the thesis prepared by Frehiwot Gashaw G/Mariam entitled: synthesis, characterization ,and fabrication based on TPA derivative sensitizer using TiO_2 nanoparticle for possible application of DSSCs devices, which is submitted to Center for Environmental Science in partial fulfillment of the requirement for the degree of Master of Science in Environmental science , compiles with the regulations of the Addis Ababa University and meets the accepted standards with respect to originality and quality.

Approved by examining board:

Name	Signature	Date
1. Dr. Yedilfana Setarge (Advisor)	_____	_____
2. Dr. Mekonnen Abebayehu (Advisor)	_____	_____
3. Dr. Kibrom G/Hiwot (Examiner)	_____	_____
4. Dr. Girum Ayalneh (Examiner)	_____	_____

Declaration

I declare that this thesis is my original work and has not been presented or submitted partially or in full by any other person for a degree in any other university, and that all sources of materials used for the purpose of this thesis have been duly acknowledged.

Therefore, I confirm that the intellectual content of this work is the result of my own efforts and prepared under the guidance of my advisors**.**

Name: Frehiwot Gashaw G/Mariam Signature: _____

This MSc. Thesis has been summited for examination with my approval as a university advisor.

Advisors: 1. Dr. Yedilfana Setarge _____

2. Dr. Mekonnen Abebayehu _____

Acknowledgement

First, May Lord Jesus and his mother are praised for protecting me, giving me the courage, it takes to finish my thesis, and intervening in each step of my life.

Next, I would like to thank my adviser, Dr. Yedilfana Setarge, for providing me with the wonderful opportunity to study on the DSSCs and for allowing me to join his group. Thank you for your excellent guidance, concern, and patience, as well as for providing an excellent environment in which to conduct my thesis.

I want to express my gratitude to thank my adviser, Dr. Mekonnen Abebayehu, for his availability, day-to-day follow-up, valuable suggestions, encouragement, and helpful talks during every step of this study.

My sincere appreciation also goes to Prof. Wendmagegn Mamo, Dr. Newayemedhin Tegegne and all members of stuff at the Department of Chemistry, Department of Physics as well as the Centre for Environmental Science.

In addition, I would like to thank Mr. Samuel Halala, General Manager of CCIIDI, Mr. Habtamu Arage, Mr. Lilay Mahmude, and the Ministry of Mines for their Sponsorship and financial support.

Finally, I would like to express my heartfelt gratitude to my beloved Ant w/o Etageng G/ Mariam for her continuous support and encouragement in handling my children. I also want to thank my son Michael and my daughter Yekoliya for their courage and patience while I was away from them. May God give them his rewards for your sacrifices!

Abstract

Solar energy is a renewable energy source that can meet the world's growing energy demand, reduce carbon dioxide emissions, and replace fossil fuel energy. However, the production costs of silicon-based solar cells are still too high for them to compete with the conventional energy sources available on the market. Dye-sensitized solar cells (DSSCs) show to be an attractive choice with the potential for lowering production costs. To increase the efficiency of DSSCs, new sensitizer development is crucial. The donor (D)-spacer (π)-acceptor (A) framework offers appropriate molecular structures for molecular design that work as efficient light harvesters, and electron injection into the semiconductors of the sensitizers has a significant effect on the DSSCs' performance. This study was conducted to synthesized, fabricated, and analyzed TPA derivative of metal-free organic dye-sensitized solar cells using a novel approach that combined computationally with the Gaussian 09 W software program to calculate the optimal structure and electron distribution of the two synthesized dye molecules using density functional theory (DFT) at the B3LYP functional and 6-31G ++ (d, p) basic set levels and experimental methods (Suzuki-Miyaura coupling reaction and Knoevenagel condensation).The dye FG_1 (4'-(diphenylamino)-[1,1'-biphenyl]-4-carboxylicacid) & FG_2 ((E)-2-cyano-3-(4' (diphenylamino)-[1,1'-biphenyl]-4-yl) acrylic acid) TPA derivative-based solar cell device offered the V_{OC}, J_{SC}, fill factor (%FF) characteristics of (0.55, 0.57) V, (3.75,13.35) mA/cm^2, and (42.81, 27.04), respectively. It was shown that solar cells made from the anchoring group carboxylic acid (FG_1) produced a PCE of 0.88 %. Similarly, devices (FG2) with a PCE of 2.10% were built from the cyanoacetic acid anchoring group due to better structural geometry, Photon absorption and efficiency have been increased by the addition of the cyanogroup and the double bond, as confirmed by UV-Vis's absorption, NMR and FTIR spectra. Based on the various anchoring groups, energy gaps showed that the studied molecules' energy gaps, FG_1 and FG_2, are 3.34 and 2.62 eV, respectively. Hence, this study showed that the cyanoacetic acid anchoring group can improve the semiconductor TiO_2 nanoparticle's efficiency and charge transfer.

Key words: DSSCs, DFT, D–π–A, TPA, TiO_2, Solar energy.

Table of Contents

List of figures

List of Tables

List of Abbreviation and Acronyms

BHJ	Bulk heterojunction
B_3LYP	Becke3-parameter Lee-Yang-Parr
CB	Conduction band
CE	Counter electrode
CIS	Copper-Indium-Selenide
C-Si	Crystalline silicon
CT	Charge transfer
DSSCs	Dye Sensitized Solar Cells
DFT	Density Functional Theory
D–π–A	Donor (D)-spacer (π)-acceptor (A)
e-	Electron
eV	Electron volt
η	Efficiency
FF	Fill Factor
FG_1	Frehiwot Gashaw one
FG_2	Frehiwot Gashaw two
FTO	Fluorine Doped Tin Oxide
HOMO	Highest occupied molecular orbital
LUMO	Lowest unoccupied molecular orbital
NIR	Near infra-red light

V_{oc}	Open Circuit Voltage
PV	Photovoltaic
PCE	Power conversion efficiency
PSC	Power solar conversion
Jsc	Short Circuit Current
TCO	Transparent Conductive Oxide
TPA	Triphenylamine
TiO_2	Titanium Dioxide
THF	Tetrahydrofuran
UV-Vis	Ultraviolet -Visible Spector-photometry
VIS	Visible light
WE	Working electrode

CHAPTER ONE

1.INTRODUCTION

1.1. Background

Energy is the heart of today's world, and has been used to enhance and sustain people's quality of life. Rising energy consumption is partly due to the increase in the world's population and technologically advanced cities (Geldasa et al., 2023). The majority of energy sources used by humankind throughout the past century have been non-renewable, with fossil fuels like oil, gas, and coal accounting for over 80% of all energy resources (B. Zhang & Sun, 2019).

When fossil fuels are becoming more limited and expensive, in addition to the harmful gases produced due to their use and damage to the environment and its people (Han et al., 2021). The problems can be addressed by using renewable energy. Finding clean, renewable, and sustainable energy sources is crucial (Kacimi et al., 2021) .Wind, hydropower, biomass, geothermal, tidal, and solar energy are examples of renewable energy sources (Bist & Chatterjee, 2021) .

Solar energy is the most practical of these sources since it is clean, plentiful, affordable, and pollution-free. The sun generates all renewable energy, either directly or indirectly (Chaudhari et al., 2020). Even when comparing other renewable energy resources with solar energy, it is clear that the potential of solar energy massively outshines that of its competitors (Aslam et al., 2020) .In one hour, the amount of solar energy that reaches our planet is enough to meet all of humanity's annual energy needs, including both heat and electricity. This impressive energy source can be converted to electrical energy using solar cell technology (Mohamed et al, 2021).

Today, one of the solar irradiance collection methods with great benefits is photovoltaic technology, which directly harvests energy from the sun (Mohamed et al., 2021) . Photovoltaic technology is a promising technology of transforming solar radiation energy into electrical energy (Weldemicheal et al., 2023). Photovoltaic technology is divided into three generations. First generation (traditional silicon solar cells), second generation (thin film solar cell technology), and third generation (emerging solar cell technology). Third generation of photovoltaic technology includes: organic solar cells, dye-sensitized solar cells (DSSCs), quantum dot solar cells, perovskite solar cells etc.(Asfaw et al., 2023).

Dye-sensitized solar cells (DSSCs) are utilizing the photo-electrochemical principle. It has an important class of photovoltaic devices. The majorities of this device are inexpensive, highly efficient, and have a wide range of device applications (Cheng-Yu Lai, 2023) . The photosensitizer is a dye molecule and has an enormous influence on the efficiency of DSSCs. There are three classes of photosensitizers that are metal complex sensitizers, metal-free organic sensitizers and porphyrin dyes complex sensitizers (Yahya et al., 2021). Among this metal-free organic sensitizers dyes can exhibit outstanding light absorption properties because they have very high molar extinction coefficients in the charge transfer band and easily tunable optoelectronic features (Driss FADILI et al . 2024).

It grasped increasing research attention recently owing to their advantages, including well-defined molecular structure, accurate molecular weight, easier synthesis and purification; easier processing compared with metal complex dyes, and in general, higher charges carrier motilities (Bayannavar et al., 2021). The purpose of this study was to synthesis, characterization, and fabrication based on TPA derivative sensitizer using TiO_2 nanoparticles for possible application of DSSCs devices. The investigation was made on NMR, UV, FTIR, Spectroscopy and JV curve characterization with solar simulator.

1.2. Statement of the problem

The 21st century needs efficient, promising technology to keep up with the growing energy sector and economics. Silicon solar cell technology dominates the commercial photovoltaic (PV) market. The cost of electronic-grade silicon wafers and highly sophisticated fabrication procedures make the manufacturing process costly. However, to lower production costs, easily manufactured materials, such as metal-free organic dye-sensitized solar cells, solve the problem. A metal-free organic dye with TPA dye is attractive for study because it facilitates efficient charge transfer upon light absorption. It is capable of absorbing diffuse light, working efficiently in cloudy climates. TPA as a donor material can be combined with a phenyl molecule as a - π- bridge and anchoring group to generate the novel design architecture, which can potentially have strong charge transfer absorption bands that harvest sunlight for photon-to-electron conversion. As the photoanode material dye-sensitized solar cell, the TPA based 4'-(diphenylamino)-[1,1'-biphenyl]-4-carboxylic acid (FG_1) and (E)-2-cyano-3-(4'-(diphenylamino)-[1,1'-biphenyl]-4-yl) acrylic acid (FG_2) has better solution to energy conversation application.

1.3. Objective of the study

1.3.1. General objective

The main objective of this study is to synthesize, characterization, and fabrication organic small molecules based on TPA derivatives with TiO_2 nanoparticles for possible application of DSSCs devices.

1.3.2. Specific objective

- To synthesize metal free based on TPA derivatives with Carboxylic and cyanoacrylic acids anchoring group.

- To characterize synthesize dyes by NMR Spectroscopy and UV-vis. spectroscopy.
- To investigate the band gap of the two dyes using an advanced computational technique by density functional theory (DFT) calculation as implemented in Gaussian 09 at 6-31++ G (d, p) level.
- To evaluate the light conversion efficiency of DSSCs cell devices using standard Keithley Type 2400A Solar Simulator.

1.4. Significance of the study

Energy demand has exponentially increased because of modernization, and this has significantly increased the energy available for the generation of energy from renewable sources. DSSCs is an advanced, environmentally friendly solution with endless potential to address the problem. Future applications of metal-free organic molecules solar cells are appealing due to their affordability, lightweight, and flexibility advantages. This study could be the basis for future computational and experimental investigations into organic molecules. The findings of this study will give information gap about various synthetic metal free organic dyes used in solar cell applications. Future experimental and computational investigations can benefit highly from the methods used in this research.

1.5. Scope and limitation of the study

The scope of the research was to synthesize and characterize the potential of the selected metal free organic molecule dye for the fabrication of dye-sensitized solar cells. The dyes are selected based on their unique advantages and have presented a wide variety of metal free organic photovoltaic materials obtained from experimental and computational analysis.

The laboratory-based experimental work encompasses different chemicals, instruments, and measurement devices, and computational investigations were done using Gaussian 09

software for the optoelectronic properties of dye molecules. The main limitation of this research is the shortage of time and the availability of funds and resources for further investigation. Like shortage of surface morphology of metal free organic molecules from various tool characterization techniques such as Atomic Force Microscopy (AFM), Transmission Electron Microscopy (TEM), and so on.

CHAPTER TWO

2. LITERATURE REVIEW

2.1. Energy demand and Supply

Energy demand globally increased significantly in the twenty-first century due to increased population and economic growth. The majority of the energy in the existing system comes from fossil fuels (Dominik Keiner, et .al, 2023). Global primary energy consumption by source has been growing slowly between 2000 and 2022, as Figure 1 illustrates. Fossil fuel consumption was responsible for 37.15 billion metric tons of greenhouse gas emissions worldwide in 2022, demonstrating how much dependence on fossil fuels can raise carbon emissions significantly, degrade air quality, and lead to supply shortages (Statista, 2024).

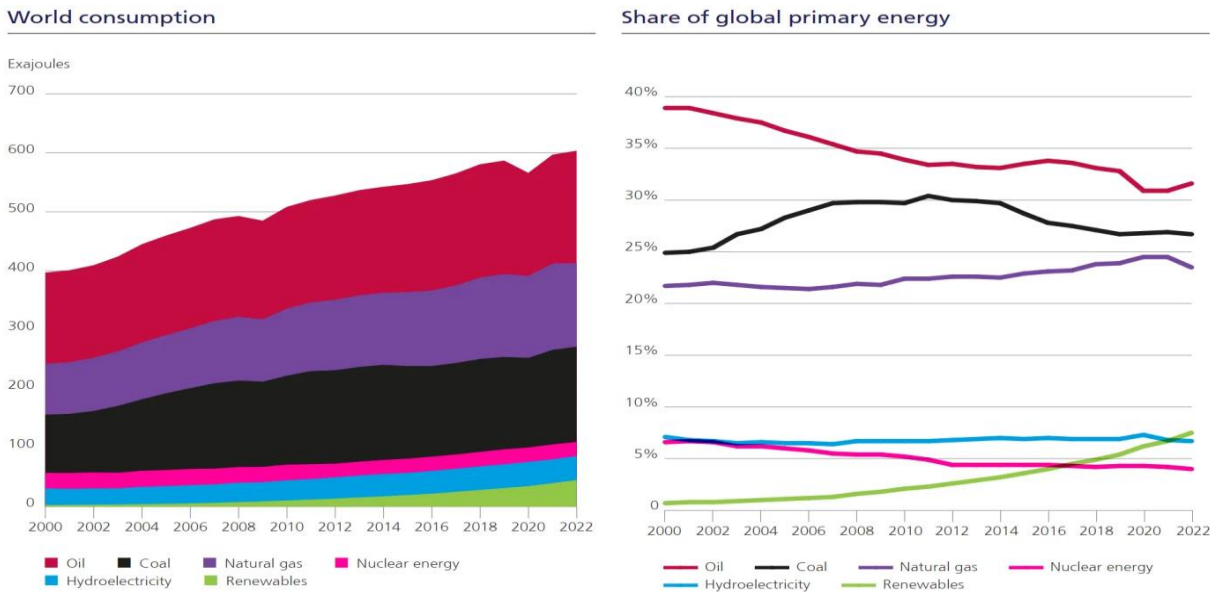

Figure 1 Global primary energy consumption by source (Source: BP Statistical Review of World Energy 2023) (https :// diesel net.com /news/2023/ 07 energy review. php)

The global energy sector has to transform how energy is produced, used, and distributed. By 2050, the amount of energy consumed globally is expected to have doubled, with electricity contributing to most of this increase compared to other energy sources (Gielen et al., 2019). Global demand for renewable energy increased by over 50% to nearly 510 gigawatts (GW) in 2023, the fastest growth rate in the previous 20 years, with capacity added annually worldwide as shown in (Figure. 1) (Energy Institute - Statistical Review of World Energy (2023).

The production, distribution, and use of energy must undergo a significant transition in the global energy sector. By 2050, the world's energy consumption will have doubled, with electricity accounting for a larger share of that growth than other energy sources (Obiora et al., 2024) . A rising portion of the world's energy has to come from renewable sources. 2023 had the fastest growth rate in the previous 20 years in terms of the amount of renewable capacity added annually worldwide, rising by about 50% to nearly 510 gigawatts (GW) (Al-Shetwi, 2022) .

2.2.Global electricity demand and production

Electricity is often associated with and widely recognized as the main driving force for the development of modern society and the worldwide expansion of national economies. Renewable energy sources are abundant and potentially beneficial, and 80% of the world's population still lives in countries that primarily rely on imported fossil fuels (by Wadim Strielkowski ,*ORCID et al., 2021).

By 2050, 90% of the electricity generated worldwide should come from renewable sources, according to the IREA. Fig. 2 illustrates this; over the five years before that, the increased by 85% (Ikpesu et al., 2020) . By 2023, the total amount of new renewable capacity added worldwide will soar to over 440 gigawatts, an astounding 107-gigawatt increase (Market, 2023). Concerns about energy security, increased support, and the affordability of solar,

wind, and energy storage all contributed to the highest percentage increase in the past ("CO_2 Emiss. 2022," 2023). The global energy crisis, the high cost of fossil fuels and power, and other factors caused inaccurate numbers. As a result, renewable energy technologies become more accessible and there is an increasing awareness of the benefits of renewable energy for energy security (Media, 2023).

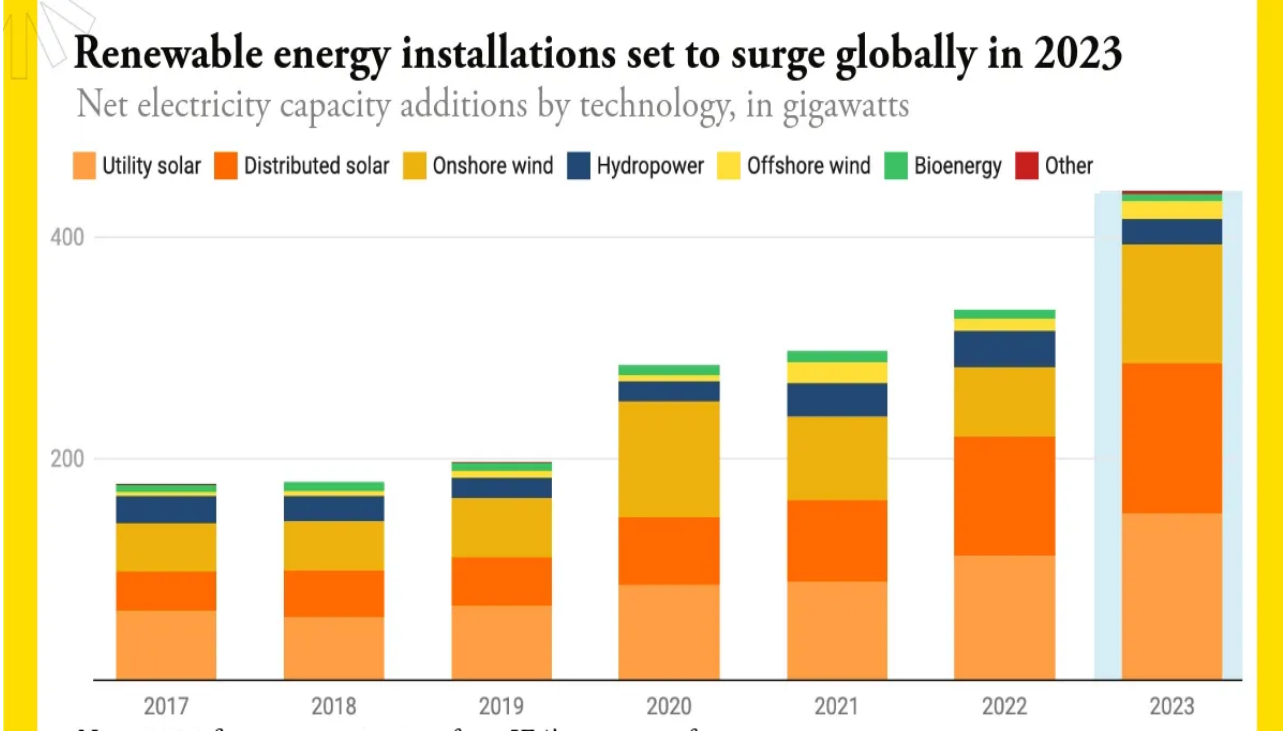

Figure 2 Global renewables developments. (Https://www.canarymedia.com >articles> clean – energy)

2.3.The solar radiation spectrum and Energy

Planck's law state that the sun emits energy at about 5880 K, acting almost like a black body (Al-Alwani et al., 2016). Nuclear fusion, which converts hydrogen into helium, is the primary driving force behind this (Taylor, 2021) . Solar radiation provides the energy that determines the Earth's atmosphere and climate. It emits radiation that extends over the

entire electromagnetic spectrum, from the highly intense X-ray region to the ultraviolet, visible, infrared, and far infrared regions (Amineh, 2020). However, 70% of the sun's energy is available between 380 and 900 nm in the visible spectrum and near-infrared (NIR). PSCs should have absorptions in this region that match the solar energy spectrum (Ansari et al., 2021).

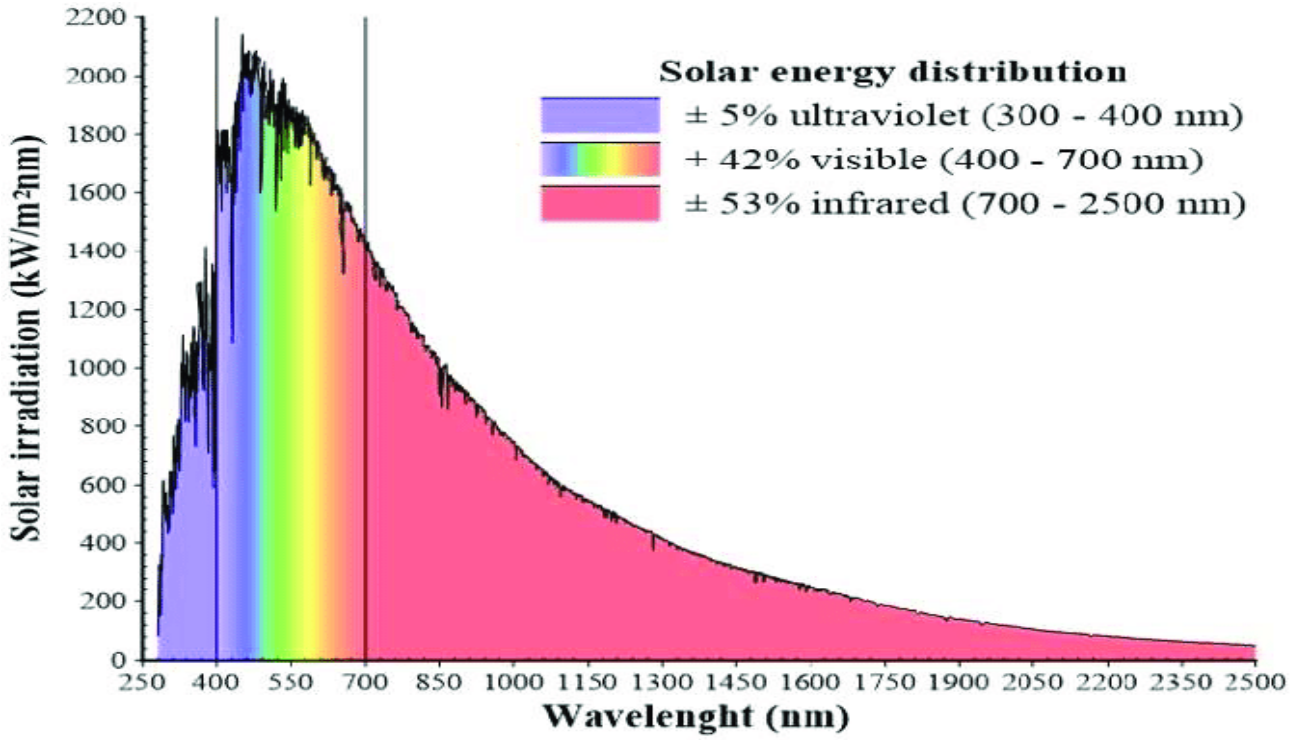

Figure 3 :Electromagnetic spectrum of the solar radiation
(http://dio.org/10.1051/e3sconf/202017221003)

2.4.Solar Energy Potential

The Sun provides around 340 W/m^2 (radiant flux per unit area, or irradiance) to the Earth when averaged globally (Rabaia et al., 2021). Solar radiation provides a free resource that could potentially be found to varying degrees anywhere on Earth as shown in the figure 4.

Solar PV power plants turn sunlight into electricity (T. Zhang et al., 2018). In the current era of global climate change and rising oil prices, PV technology provides a unique opportunity for governments and communities to alter or enhance their energy infrastructure and accelerate their low-carbon energy transition.

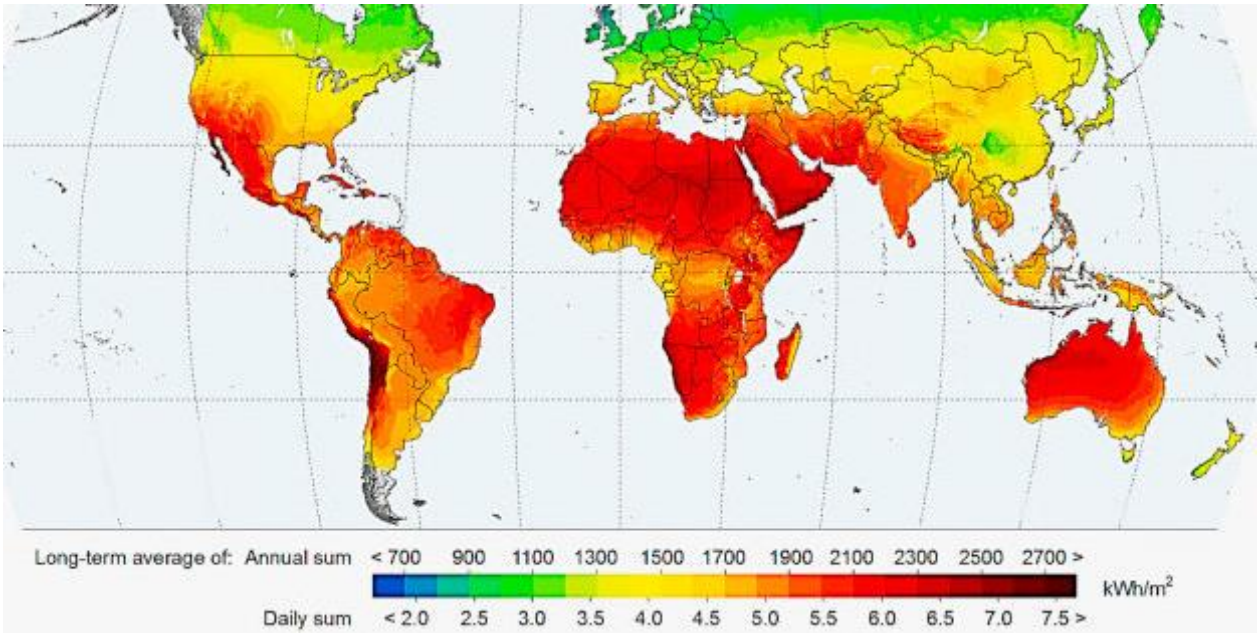

Figure 4 Global solar energy potential (Kannan &Vakeesan,2016)

2.5.Solar Energy potential in Ethiopia

Ethiopia is a country in Sub-Saharan Africa, located at 3–15°N latitude and 33–48°E

longitude. The country receives a lot of solar energy because it is located in the tropics. Ethiopia covers 1.13 million square kilometers of land (Anshebo et al., 2023)(Getachew Alemu & Alemu, 2021).The annual average daily solar radiation reaching the ground is predicted to be 5.5 kWh/m^2/day, ranging from 4.5 kWh/m^2/day in July to 6.5 kWh/m^2/day

in February and March. This broad spectrum of radiation potential can be harnessed and utilized for the best economic development (Hailu & Kumsa, 2020) as shown in figure 5.

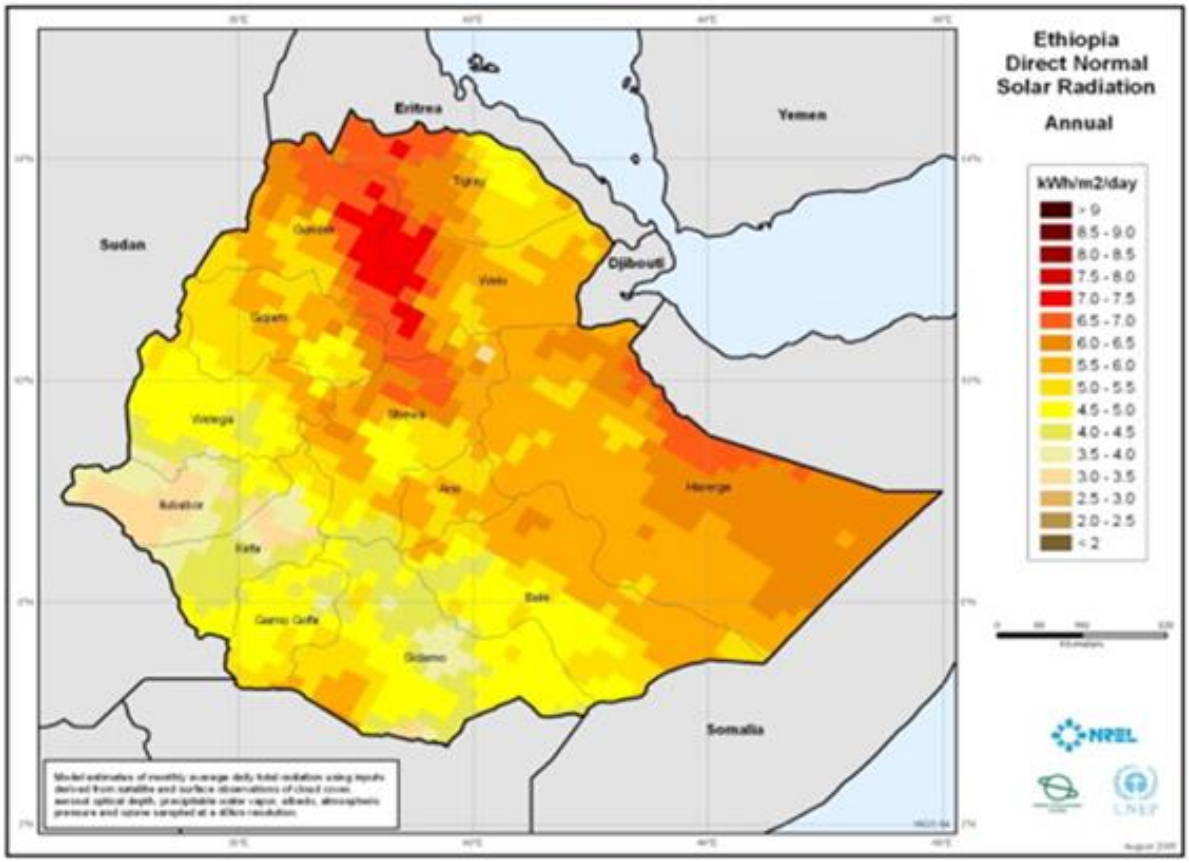

Figure 5 Solar resource map in Ethiopia. (http://dx.doi.org/10.1016/j.seta.2015.02.003)

2.6.Generations of solar cells (Photovoltaic)

Solar energy, which is increasingly gaining popularity, is the most practical, environmentally responsible, and long-lasting alternative source of renewable energy(Weldemicheal et al., 2023). Humanity could have everything it needs to harness this massive solar influx. There is a widespread belief that solar energy has enormous potential for future power production. Photovoltaic technology is a promising way to turn

solar radiation energy into electrical power (Han et al., 2021). PV cells are composed of materials related to semiconductors, exhibiting optimum electrical characteristics. Developing materials with such characteristics leads to the establishment of different generations of solar cells, as shown in figure 6.

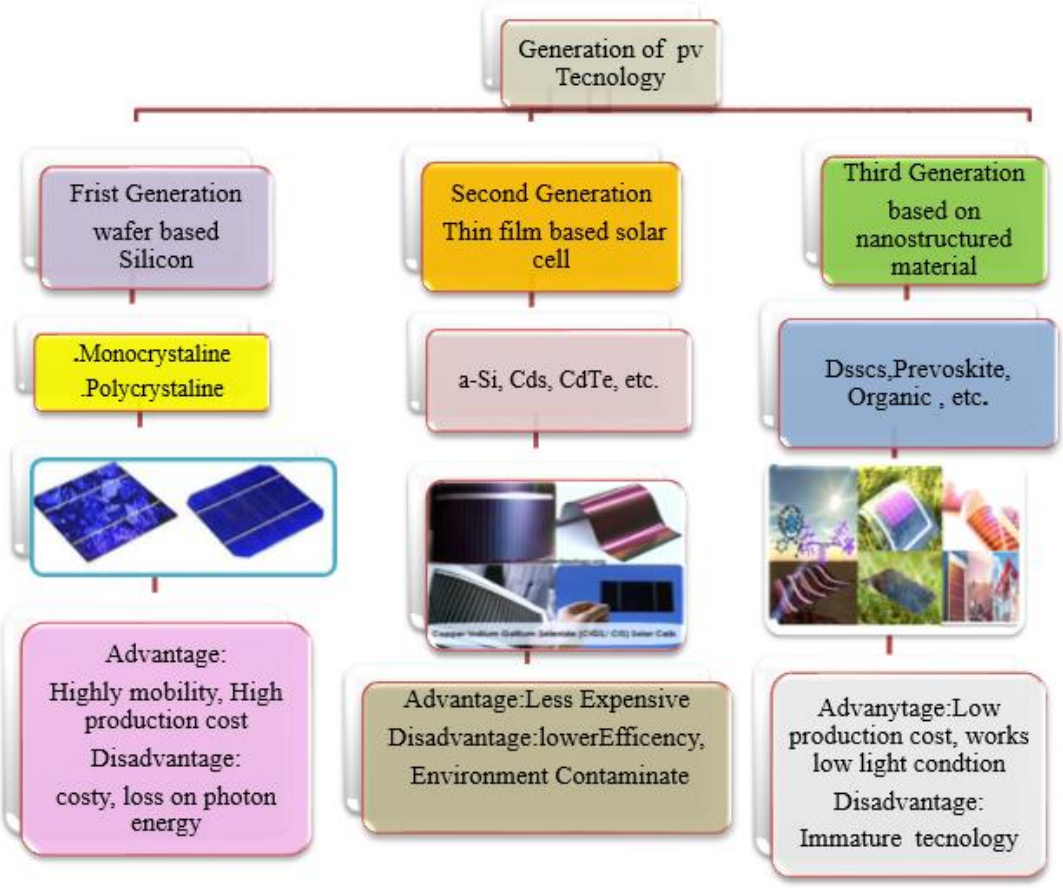

Figure 6 Solar cell technology generation

Wafer-based and thin-film solar cells are two categories of PV technology. They differ from one another in terms of light absorption, energy conversion, production process, and cost (R. Vinayagamoorthi et., 2023). Wafer-based cells are built on semiconductor wafers and used without a separate substrate, even though components utilize glass for mechanical stability and protection. Slices of semiconducting wafers made from alloys make these cells (B. P. Prem Singh Saud et.al, 2024).

Thin-film cells utilize insulating substrates like glass or flexible plastics. Thin films can also classify into commercial and emerging thin-film technologies (Jean et al., 2015). There are three types of generation of solar cells. The first, second, and third generation.

2.6.1. Wafer-based solar cell

First generation solar cell generations technologies consist of wafer-based solar cells are made of materials like crystalline silicon (c-Si). Crystalline silicon (c-Si) PV cells are the leaders in the global photovoltaic market and are the most developed PV technologies. Mono- or poly-crystalline silicon wafers are the building blocks of silicon solar cells (Karim et al., 2019). Due to their highest power efficiency, silicon-based solar cells now account for more than 80% of the installed capacity worldwide and have a 90% market share.

The highest reported energy conversion efficiencies in the lab for mono-crystalline and poly-crystalline solar cells are 26.7% and 22.3%, respectively (Bayannavar et al., 2021). Polycrystalline silicon is more durable than mono crystalline silicon. However, the lower cell efficiency compensates for the reduced manufacturing cost. The drawback of the first-generation solar cell's higher cost overcomes its higher efficiency (Prem Singh Saud et.al, 2024). These resulted in a need to eliminate unnecessary material, particularly in the active layer, which motivated the development of thin film second-generation solar cells (Prem Singh Saud et al.,2024). This generation maintained the appropriate cell efficiency while using less material. The thin-film solar PVC technique uses a photoactive layer between 1 and 10 micrometers thick and is more effective than C-Si at absorbing solar energy (Ajay Jain et al ., 2024).

2.6.2. Thin-film based solar cells

The two main categories of thin-film solar cells are commercial and emergent or novel thin-film technology: -

2.6.2.1.Commercial thin-film solar cells

The three most common thin-film solar cells used in the commercial are cadmium telluride (CdTe), amorphous silicon (a-Si), and cadmium sulfide (CdS). This advantage of these materials is due to their use of cheaper raw resources and less costly manufacturing processes (Ramanujam et al., 2020). For instance, reducing manufacturing operations may produce thin-film modules in a highly automated and streamlined way, resulting in modules with low per-watt costs. Compared to their silicon counterpart, they are easier to handle, more flexible, and less prone to breakage.

Amorphous silicon is preferred over other materials in thin film technologies, such as CdS/CdTe, because of its efficiency. Non-crystalline amorphous silicon (a-Si) cells have a silicon extract-containing thin film structure. The effectiveness of light harvesting is 40 times greater in amorphous silicon (Subhasri Kar et al , 2023). These benefits are amorphous silicon materials, making them more widely available and economical. It's due to the need for a layer that is smaller in a photovoltaic thin film cell.

2.6.2.2. Emerging or novel thin-film solar cells

The emerging thin-film solar cells include dye-sensitized solar cells (DSSCs), organic photovoltaic, perovskite, quantum dot photovoltaic (QDPV), and copper zinc tin sulfide (CZTS) (Ikpesu et al., 2020). These technologies are the result of intensive research and development work in the fields of device engineering and material discovery (Ikpesu et al., 2020).DSSCs differs from other types of thin-film solar cells in terms of sensitizers and layer structure. Recently, interest has increased in the dye-sensitized solar cells (DSSCs), which Grätzel and his colleagues developed in 1991(Asfaw et al., 2023).

To improve the photovoltaic performance of DSSCs, a variety of sensitizers have been created, which can be divided into metal complex sensitizers and metal-free organic sensitizers (G. Sharma et al., 2023). Metal complex sensitizers (inorganic based solar cell) are a limited and expensive resource. Organic photosensitizers that are metal-free are in

high demand in order to obtain even less expensive photosensitizer for DSSCs (A et al., 2021). Metal free complex sensitizers dyes provide exceptional cheap cost, lightweight, and great mechanical flexibility, as well as molar extinction coefficients, environmental friendly , and a wide range of molecular architectures (Khalida Abaid Samawi et. al ,2022).

2.7. Improving solar cell efficiencies

The 1950s prompted an attempt to commercialize silicon photovoltaic cells in geographically isolated areas away from the electrical grid. The first silicon solar cell that was useful was created by Bell Laboratory, and it had an efficiency of more than 5%; currently, the best solar cells have an efficiency of over 40% (Węgierek, 2022).Over the years, many materials and device structures have been studied, and there are continual advancements such as single-crystal silicon, multi-crystal silicon, copper indium gallium selenide (Cu (In Ga) Se_2), cadmium telluride (CdTe), and multiple types of organic solar cells in bulk and thin film with a single junction and multi-junction structure (Kettle et al., 2022).

The most advanced materials for commercial products of solar cell applications are based on silicon, and GaAs have an efficiency of just over 20%, although device efficiency has increased dramatically over the past several years (Popoola, 2023). DSSCs are introduced recently but, are not well commercialized yet due to their low efficiency. Silicon cells lead the terrestrial solar cell market because of their relatively lower cost. The effectiveness of the first cell was only 7%, according to O'Regan and Grätzel; however, with the assistance of Grätzel's team, it increased to about 10% (Kamal Prajapat et .al ,2023). The data chart from the National Renewable Energy Laboratory shows the highest certified conversion efficiency for research cells across a range of current solar technologies.

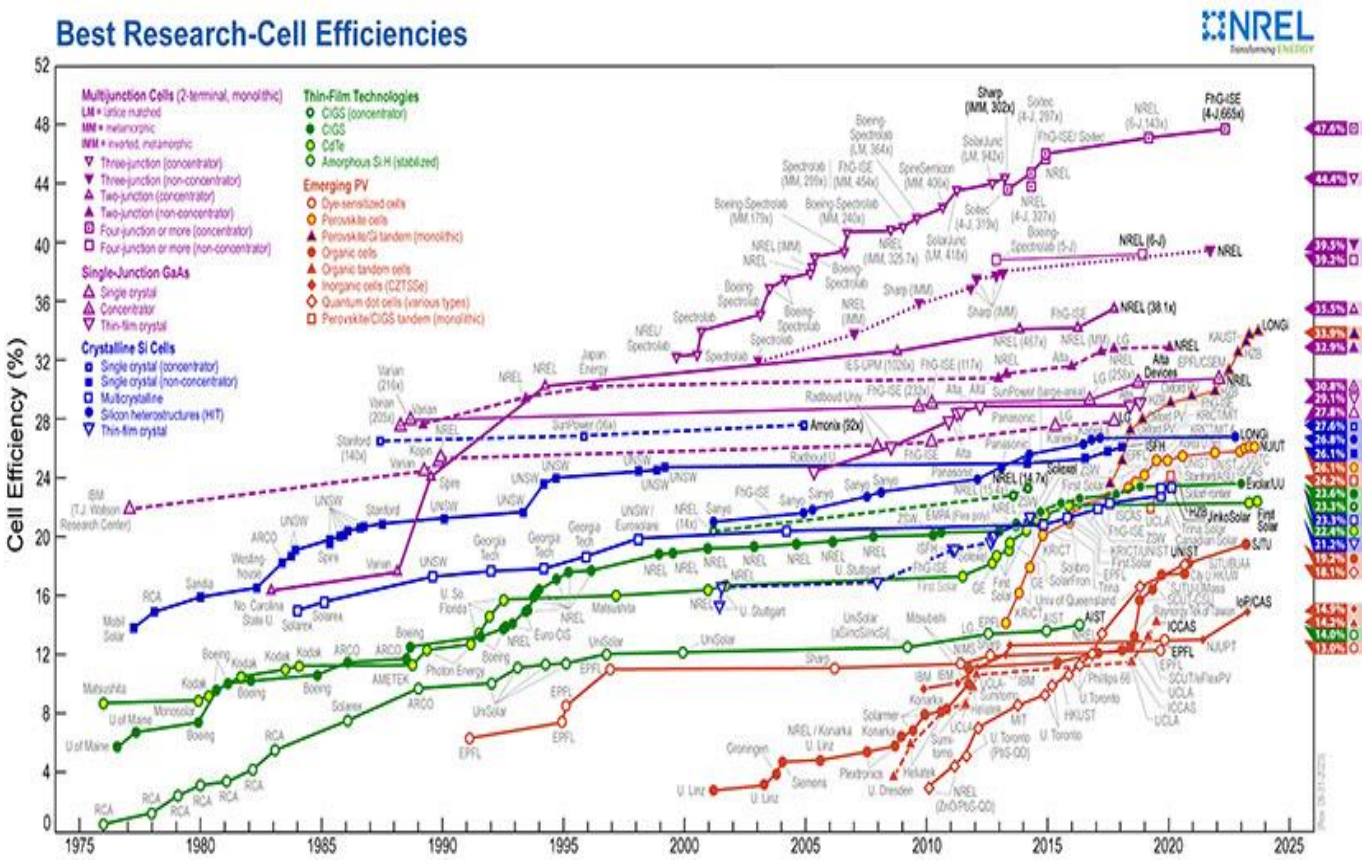

Figure 8 Figure 8 The National Renewable Energy Laboratory (NREL) reported various solar cell technologies to this chart, all of which achieved high cell efficiencies between 1976 and 2025. (https://www.pv-magazine.com/2024/04/24/nrel-updates-interactive-chart-o

On the laboratory scale, the highest certified result recorded is 13% (Alfred Błaszczyk et.al, 2021).The scientific and industrial communities have shown interest in the use of DSSCs materials in solar cells because of their low cost, lightweight, and ability to be incorporated into flexible, large-area devices to meet the market's growing need (B. P. Prem Singh Saud et.al , 2024). As shown in Figure 7, the National Renewable Energy Laboratory of the U.S. Department of Energy is combining the progress in various solar technologies over the past 40 years into a single graph (Editors@pv-magazine.com., 2024).

2.8. Components of Dye-Sensitized Solar Cell

Among the third generation of photo-electronic devices are dye-sensitized solar cells. In 1991(Berry, 1991), O'Regan and Grätzel developed DSSCs , a novel type of third-generation solar cell . They are colorful, transparent, and flexible. As a result, DSSCs are regarded to be among the most promising next-generation technologies for satisfying energy demands and environmental remediation in the future (B. P. Prem Singh Saud et. a1,2024). DSSCs comprises mainly of five parts which include a substrate, photo electrode, sensitizing dye, electrolyte and counter electrode (Ikpesu et al., 2020) as shown below in the figure 8.

2.8.1. Transparent Conductive Substrates

DSSCs are typically made from two sheets of transparent conductive material, which serve as both current collectors and substrates for depositing catalysts. (Ikpesu et al., 2020). The two basic characteristics of the substrate used in DSSCs are: First, the substrate must be more than 80% transparent to allow the best sunlight to reach the active area of the cell. Second, it must have high conductivity for efficient charge transfer and low energy loss in DSSCs (K. Sharma et al., 2018).

Fluorine and indium doped tin oxide (FTO, SnO_2: F and ITO, In_2O_3: Sn, respectively) are commonly used as conductive substrates in DSSCs. In comparison to ITO, FTO has been shown to have greater thermal stability. Sima et al. reported that following thermal annealing at 450 ^{0}C, ITO's sheet resistance can increase from 18 Ω / cm^2 to 52 Ω / cm^2 while FTO's stay remains constant (Ikpesu et al., 2020). FTO is better suited than ITO for interlayers that need a high annealing temperature, like titanium dioxide. Furthermore, FTO is better developed than ITO and is more commonly available on the market. FTO has a lower sheet resistance (7-8 Ω / cm^2) (Ruba et al., 2021).

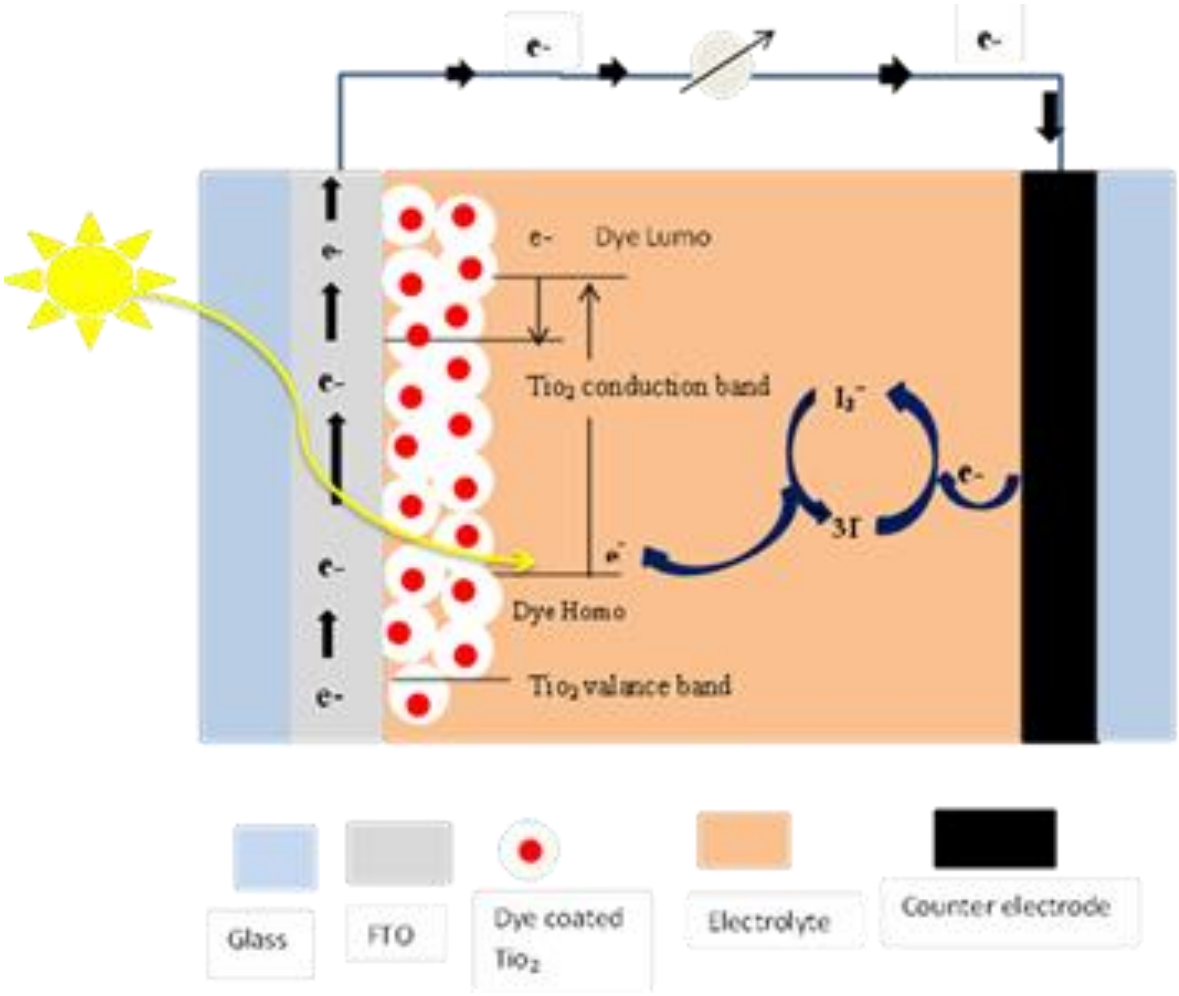

Figure 9 Schematic representation of dye sensitized solar cell

.

2.8.2. Mesoporous Semiconductor oxide.

The semiconductor oxide absorbs the electrons from the active dye and sends them to the external circuit to generate an electric current. Semiconductors provide a surface for dye binding. The crystallinity, morphology, and surface area of the semiconductor has a significant impact on the electron transport rate, which determines the efficiency of the DSSCs (Kamal Prajapat et .al , 2023).

In the past, metal oxides such as zinc oxide, titanium oxide (TiO_2), and others have been used as semiconductor materials (Phuti S. Ramaripa et.al, 2024). Compared to other metal oxides, TiO_2 is an attractive material for technological applications due to its versatility, abundance, low toxicity, chemical stability, light sensitivity, and photo stability.

Titanium oxide (TiO_2) has been shown to have the highest experimental DSSCs performance. Because it has a higher conduction band boundary energy (3.2 eV) than either of the other two forms (3 eV), anatase was chosen as the preferred TiO_2 crystal form over rutile (Hira Kanwal et.al , 2024). The chemical stability of anatase results from its high band gap energy. The electron transport mechanism moves more slowly in rutile because it is denser than anatase (Phuti S. Ramaripa el. al, 2024).

2.8.3. Sensitizing dye (photosensitizers)

The photosensitizer is a dye molecule and has an enormous influence on the efficiency of DSSCs. An effective photosensitizer should:

(i) Exhibit strong absorption in the visible spectra (400 nm to 700 nm) including the infrared spectra,

(ii) It must be strongly connected to the semiconducting oxide with the proper anchoring group as carboxylic or hydroxyl group,

(iii) Have a high extinction coefficient,

(iv) Be stable in its oxidized form so that it can be reduced by an electrolyte

(v) Possess a more positive HOMO than the redox potential of the electrolyte and a more negative LUMO than the CB of the semiconductor.

There are three classes of photosensitizers are metal complex sensitizers, metal-free organic sensitizers and porphyrin dyes complex sensitizers (Ikpesu et al., 2020).

2.8.3.1. Metal complex sensitizers

Metal complex sensitizers have a central metal ion, auxiliary ligands, and at least one anchoring ligand. Auxiliary ligands can be used to tune the overall properties of the complex even when they are not physically attached to the semiconductor surface (Conradie, 2024) . The adsorption of the complex to the semiconductor surface is due to the anchoring ligands, which are chromophores. The main metal ion in the center greatly affects the overall properties of the metal complex. Ruthenium compounds, which are the most effective and have been extensively studied, are the most widely used metal complex photosensitizers due to their higher absorption capacity. In the visible area, of the spectrum due to the charge transfer of the metal-ligand. Single state (Neeraj Tomar et.al, 2020).

The electro-spray ability of these dyes is excellent and their stability is high. Ru-based dyes have conversion efficiencies greater than 10% (B. P. Prem Singh Saud et.al, 2024), although they are typically prepared using multistep and time-consuming chromatographic techniques. In addition, they also have low molar extinction coefficients and small near-infrared absorption spectra. However, Ru (II) has several disadvantages, including high price, rarity, toxicity, and difficulty in synthesis (G. Sharma et al., 2023).

2.8.3.2. Metal free complex sensitizer

In comparison to metal complexes built on Ru (II) dye, organic dyes without metal have a number of advantages (Liu et al., 2021). Without any resource limitations, it is inexpensive to synthesize metal-free organic colors. These dyes can exhibit outstanding light absorption properties because they have very high molar extinction coefficients in the charge transfer band and easily tunable optoelectronic features (Han et al., 2021). However, as compared to devices designed with dyes based on ruthenium, the efficiency of these sensitizers is still Organic photosensitizers made without metal are constructed disadvantaged. Nevertheless, by carefully choosing or fine-tuning the design components, efficiency and performance can be increased using the D - A, D- π - A, D- π –A -A, and other designs. A is an acceptor, is a conjugated bridge, and D is a donor (Kashish Virendra Sagar et.al, 2024).
The D- π -A method offers adaptable dye patterns that are easily tweaked to produce appropriate dye characteristics. The photo physical properties of the dye D–π–A are related

to the intermolecular charge transfer from the donor group to the acceptor group. This transition produces a high molar extinction coefficient (Liu et al., 2020). Expansion of the π-conjugate system by adding electron donor or withdrawing groups can induce a change in the HOMO and LUMO energy levels, leading to a change in optical properties.

This means that the dye can be modified and is therefore considered a promising metal-free organic dye for DSSCs (Han et al., 2021). The dye D−π−A photo physical characteristics are related to the intermolecular charge transfer from the donor group to the acceptor group (Periyasamy et al., 2021). The molar extinction coefficient is high because of the transition. The HOMO and LUMO energy levels can alter as the π-conjugate system is expanded by introducing electron donor groups or withdrawing them, changing the optical characteristics. Because of the dye's flexibility, it is considered as a promising metal-free organic dye for DSSCs.

2.8.3.2.1. Triphenylamine base dyes for dye sensitized solar cells

Different donor groups, such as triarylamine, indoline, carbazole, phenothiazine, and coumarin etc., were included in the molecular structures of the metal-free organic sensitizers to absorb the photons and facilitate the charge transfer from the sensitizer to the photo anode (Yahya et al., 2021).

Triphenylamine-based dyes come out among the donor group because they are excellent electron donors and hole transporters and exhibit planarity at the central nitrogen and the three adjacent nitrogen-carbon bonds (Cheng Jih, 2024). The unbounded core nitrogen electron pair is continuously conjugating with the surrounding arm.
TPA is an attractive choice for developing dye-sensitized solar cell technology because of its excellent stability, high photoluminescence efficiency, and good solubility (Anuj Tripathi et.al, 2022)

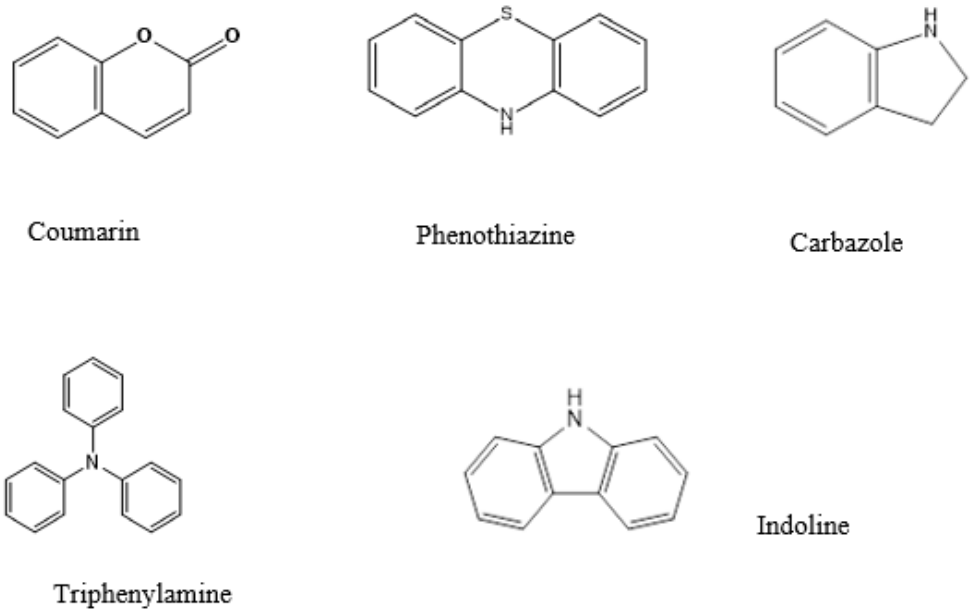

Figure 10 Molecular structures of most common electron donor

Within the donor group, aryl amine derivatives in general, such as triphenylamine (TPA), are excellent building blocks for producing electroactive material for optoelectronics applications. It resists aggregation mainly because of its higher electron-donor capacity and nonplanar shape (Devadiga et al., 2021). Due to the TPA-based dyes' reduced tendency to aggregate, excited dye molecules can quickly inject electrons into the conduction band at the interface.

In addition, TPA's propeller-like molecular structure makes it possible to prevent the interaction between the injected electrons and the redox couple (Hosseinnezhad et al., 2020). The oxidized TPA unit is also spatially positioned in an arrangement that makes it easier for the redox couple species to approach, which leads to quick dye regeneration. TPA's extraordinary stability is one of the primary reasons why researchers are interested in creating metal-free sensitizers (Han et al., 2021).

2.8.3.2.2. Anchor group

DSSCs almost exclusively employ covalent bonding between the dyes and the TiO_2 surface atoms in order to ensure strong coupling, a homogeneous dye distribution, and device stability showed high conversion efficiencies (B. P. Prem Singh Saud et. al,2024). Carboxylic acid and cyanoacrylic acid groups are most frequently used for DSSCs dyes. Among anchoring modes, bidentate modes (chelating or bridging) are the most studied, and usually the intimate contact between carboxylate anchor-based dyes and the metal oxide surface, the structure exhibits superior stability compared to other types of anchoring modes (Suryapratap J. Sharma et.al, 2023).

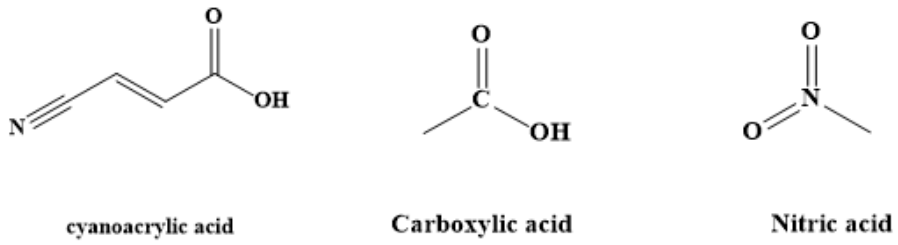

Figure 11 : Molecular structures of most common anchor group

2.8.3.2.3. Linker group

Electron rich - π - conjugated moieties serve as the linking groups for the DSSCs dye. The link group has two functions:

1) Increasing the physical distance between the dye component and the TiO_2 substrate reduces the chance of charge recombination from the TiO_2 to the oxide dye.

2) It increases the length of the conjugated chain between the dye mobility and the electron acceptor (anchor) group, both enhancing and shifting light absorption to longer bath wavelengths.

Many functional units have been used, including vinyl, alkynyl, benzene, and others.

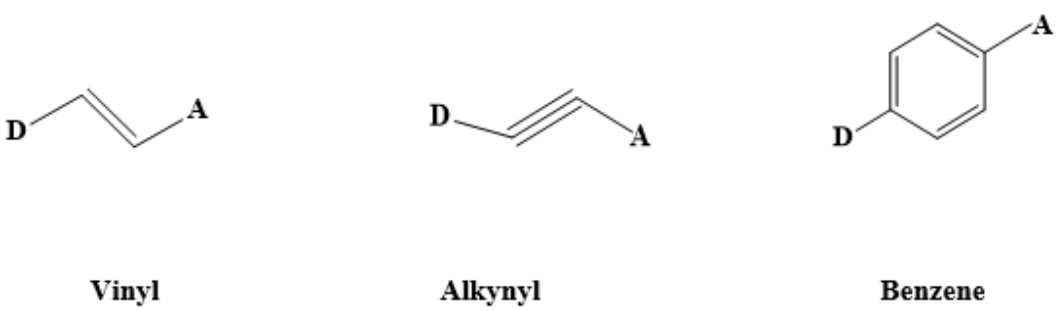

Figure 12 : Molecular structures of most common Linker group

Therefore, the proposed sensitizer carries triphenylamine chromophores of the TPA type. Benzene was chosen as the - π -linker, attached to the anchor dye on the surface of TiO_2 nanoparticles.

2.8.3.3. Porphyrin dyes complex sensitizers

The third sensitizers are large-aromatic molecules, such as porphyrin dyes, which are appealing potential candidates for thin, affordable, efficient DSSCs due to their low cost, straightforward manufacturing process, excellent molecular stability, suitable energy levels, efficient electron transfer, intense absorption (Kamal Prajapat et.al, 2023). Porphyrins exhibit strong visible-band emission and absorption, together with changing redox potentials (M. Y. A et al., 2021).

Self-assembled porphyrin molecular structures are essential to solar energy research because solar energy is efficiently captured and converted into chemical energy by porphyrin-based chromophores in the photosynthetic systems of bacteria and plants (M. M. A. M. A, 2020).

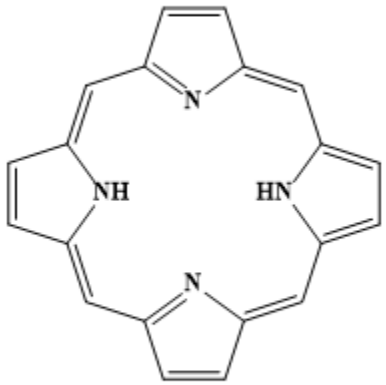

Porphyrin

Figure 13 Molecular structures of Porphyrin

2.8.4. Electrolyte

Electrolyte is a crucial component in the DSSCs, for both dye regeneration and the completion of electron transport between the photoelectrodes and counter electrode.

The electrolyte must possess the following qualities:

(i) High electrical conductivity;

(ii) Good interfacial contact with the nanocrystalline semiconductor and counter electrode;

(iii) No tendency to cause desorption or degradation of the dye; and

(iv) No visible light absorption.

Most frequently, iodide/triiodide redox couple Electrolyte was investigated in DSSCs. Whether decrease redox potential of electrolyte to increase open circuit current. Redox couple based liquid electrolyte is widely used in DSSCs especially the iodine redox couple based liquid electrolytes have been produced high photocurrent efficiency (B. P. Prem Singh Saud et.al,2024).

2.8.5. Counter electrode (CE)

The Counter electrode (CE), an essential component of the DSSCs, reduces the substances that go through redox processes and serve as intermediaries for renewing the sensitizer (dye) following electron injection (Muchuweni et al., 2020). Triiodide is created during dye molecule regeneration, and at the counter electrode, it is reduced to an iodide ion (Aslam et al., 2020). Due to its high catalytic activity and stability, platinum and 8HB pencil-based carbon are chosen as the counter electrode materials (Prem Singh Saud et.al, 2024).

2.9. Working Principle of Dye-Sensitized Solar Cells

DSSCs differ structurally from conventional solar cells due to the molecular devices and nanomaterials they contain. Four fundamental processes make up the DSSC's working principle: light absorption, electron injection, carrier transportation, and current collection (B. P. Prem Singh Saud et.al, 2024). The process that converts photons into current (as seen in Figure. 13, involves the following steps:

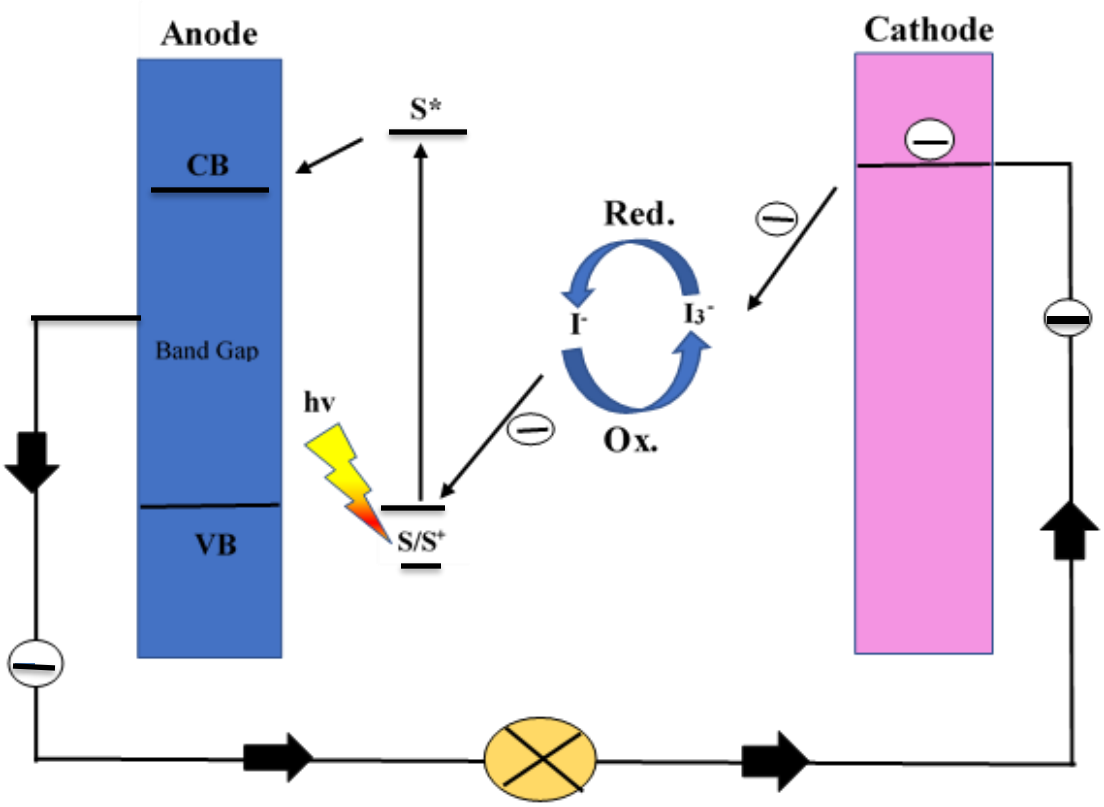

Figure 14 Schematic diagram of the DSSCs working principle

When light strikes a dye-sensitized solar cell , the dye molecule, which is initially in its ground state (S), absorbs an energy-containing incident photon (hv) and is excited to a higher energy state (S*).as illustrated in eqn (1):(Conradie, 2024)

$$S + hv \longrightarrow S^* \quad \ldots\ldots\ldots\ldots (1)$$

The excited dye molecule is oxidized, as illustrated in below equation, where S^+ is the oxidized dye molecule. Hence, an electron is injected into the semiconducting oxide film's conduction band, where it is free to flow to the external circuit through a transparent conducting electrode: (K. Sharma et al., 2018)

$$S^* \longrightarrow S^+ + e^- (TiO_2) \quad \text{..... (2)}$$

On the other hand, the oxidized dye molecule is regenerated back to its ground state by electron donation from the I^- in the redox couple, as illustrated in below:

$$S^+ + 3I^- \longrightarrow 2S + I_3^- \quad \text{..... (3)}$$

Eventually, the circuit is completed through I^- regeneration, via the reduction of I_3^- at the counter electrode, by electron donation from the external circuit, as illustrated in below:

$$I_3^- + 2e^- \longrightarrow 3I^- \quad \text{..... (4)}$$

As a result, without undergoing any chemical transformation, solar energy can be continuously converted into electrical energy by repeating these steps. As a result, in a DSSCs, charge generation occurs at the interface between the semiconductor and dye, and charge transport travels over the electrolyte and semiconducting oxide layer to and from the external circuit by the transparent conducting electrodes and counter electrodes, respectively (Job et al., 2020).

2.10. Photovoltaic parameters

The performance of DSSCs is usually evaluated by the open-circuit voltage (V_{OC}), the short-circuit current (J_{SC}), the fill factor (FF), and the PCE. These parameters are determined from the I–V plot (B. P. Prem Singh Saud et.al, 2024) . Figure 14 shows typical I–V plots for photovoltaic devices. Descriptions of these parameters are given below:

Short circuit current (J_{SC}): It is the cell maximum current measured at an applied potential of zero volt. In other word, there is no power produced at this point. The higher the short circuit current, better is the cell. The unit area short circuit current is represented by short circuit current density, whose unit is mA/cm^2 or A/cm^2 (Conradie, 2024).

Open-circuit voltage: (V_{OC}): It is the cell maximum voltage that a solar cell produces when current in the cell is zero. The higher the Voc, the better is the cell.

The fill factor: (FF) is defined as the ratio of the maximum power from the solar cell to the product of V_{OC} and J_{SC}. The FF is an important parameter that determines the PCE of an DSSCs. Graphically, the FF is a measure of the "squareness" of the solar cell and is the area of the largest rectangle that will fit in the J–V curve. Mathematically FF defines as: (Lichun Sun, Dr. et.al, 2023)

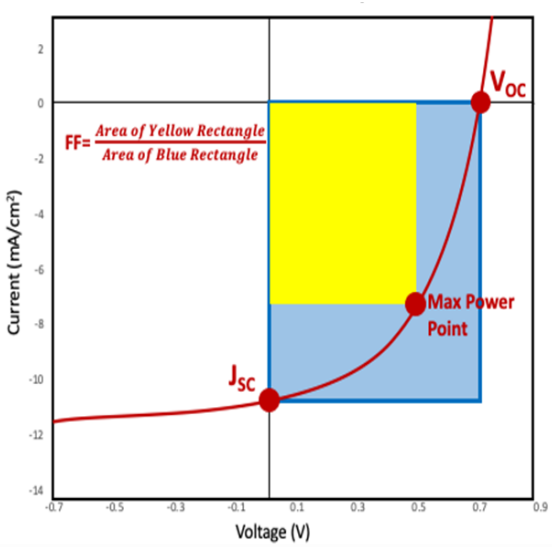

Figure 15 A current-voltage (J-V) measurement with an air mass (AM) 1.5 G spectral shape and an incident light power intensity of 100 mW cm^2 is a standard procedure to assess a solar cell's performance. (https://commons.wikimedia.orgnic photovoltaic.)

$$FF = \frac{Pmax}{Jsc * Voc} \qquad \text{..... (5)}$$

Where P_{max}, J_{SC}, V_{OC}, and FF are the maximum power output, short-circuit current density, the open-circuit voltage, and fill factor, respectively.

Power conversion efficiency (η)

Power conversion efficiency represents the efficiency of how much Incident light can be converted to electricity. It is defined as the percentage of input irradiation (P_{in}) that is converted into the output power and expressed as the product of V_{OC}, J_{SC}, and FF divided by the input power (P_{in}) (Job et al., 2020).

$$\textbf{PCE (η)} = \frac{FF(V0C * Jsc)}{P\text{in}} \qquad \text{..... (6)}$$

Where J_{SC}, V_{OC}, FF, and P_{in} are the short-circuit current density, the open-circuit voltage, the fill factor, and the input power, respectively.

2.11: Density Functional Theory

In DFT, a model known as electron density can be used to determine the interactions between the electrons and the nucleus. The probability of finding an electron in space is known as electron density (Hong Jiang, 2023). Basically, many-body wave functions depend on all spatial coordinates of all electrons, whereas electron density only depends on three spatial coordinates as shown in figure 16. Consequently, electron density is a

desired computational characteristic of DFT and offers an easy method to solve the Schrödinger problem (Ayalew, 2022).

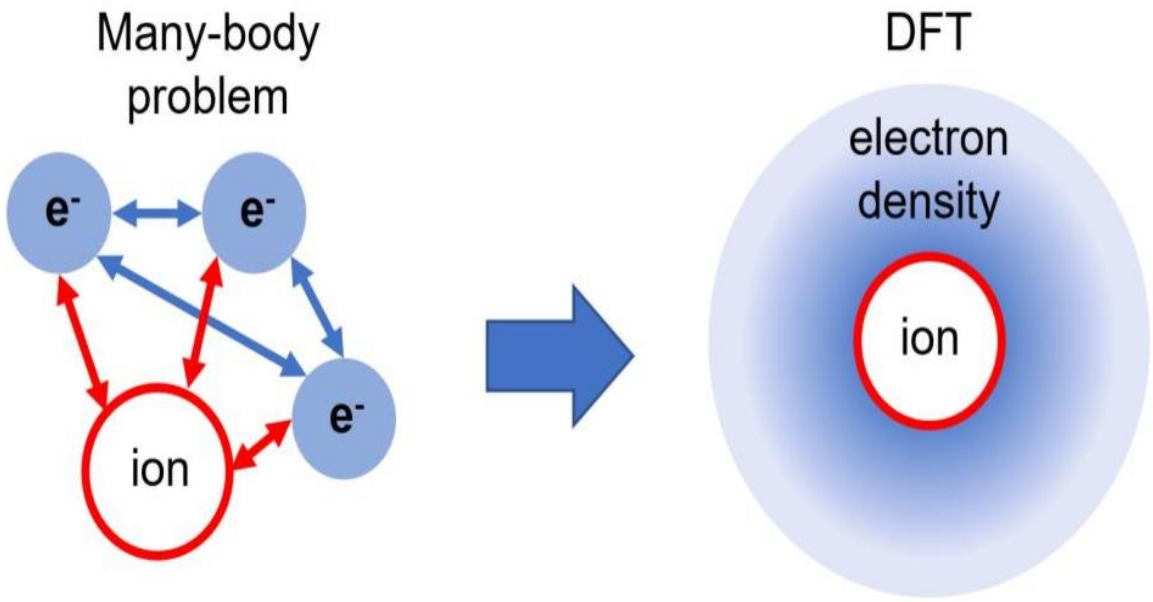

Figure 16 Difference perspective of the density functional theory versus the reality for the many-body system.

The overview of a variety of molecular properties, such as the energy of the Lowest Unoccupied Molecular Orbital (LUMO) and the Highest Occupied Molecular Orbital (HOMO), as well as the molecular shape, vibrational frequencies, thermochemistry, and energy of the optimized geometric structure of the molecule, is nearly achieved by DFT (Hong Jiang, 2023).

Density functional theory was used for DFT calculations using the Gaussian 09 package, the Becke gradient corrected exchange functional, and the Lee-Yang-Parr correlation functional with three parameters (B3LYP) approaches. The base set employed in this investigation was 6-311++G (Ahmed Azaid† et.al, 2022). Many materials scientific

applications, including surface science and catalysis, structural metals and earth sciences, semiconductors, nanotechnology, and biomaterials, are perfectly suited for computational work based on DFT. DFT applications enhance material properties and accelerate design processes by using a variety of computational approaches (Driss FADILI et. al, 2024).

2.12. The Suzuki-Miyaura cross-coupling reaction

The synthetic dyes used in DSSCs devices can be produced through organic synthesis using many types of cross-coupling reactions catalyzed by transition metals, including the Suzuki, Still, and Negishi reactions (Zani et al., 2019), etc.

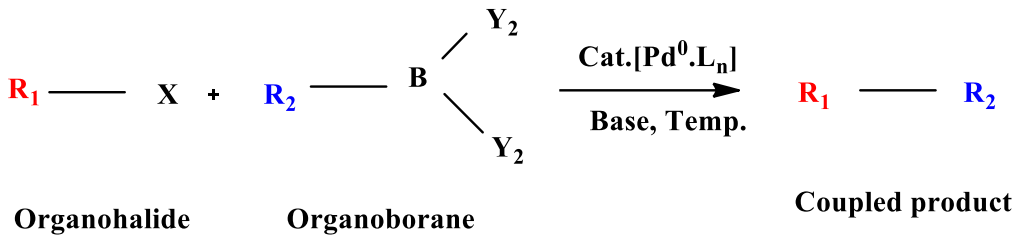

R_1 = alky,alkynyl,aryl,vinyl,benzyl R_2 = alky,alkynyl,aryl,vinyl,

X = Br,Cl, I ,OTf,OTS..... Y = $OH,(CO)_2,(CH_3)_4$ L = dba,OAc,pph_3

Figure 17 General reaction scheme for the Suzuki coupling reaction

The Suzuki reaction is superior in terms of reaction condition and it is a highly versatile method the formation of C - C single bonds (D'Alterio et al., 2021). The main advantage of this reaction is its application in the presence of various fictional groups such as esters, carboxylic acids, aldehydes etc. The Suzuki coupling mechanistic follows a catalytic cycle three primer steps. These are oxidative addition, trans metallation and reductive elimination.

I. Oxidative addition step

The oxidation of the catalytic palladium take place. It is oxidized from palladium (0) to palladium (II) with the palladium catalyst (Mehran Farhang et. al,2022). The product formed in this step is an organ palladium complex where the carbon - halogen bond is broken and the palladium inserts itself between the R group and the halogen (Zani et al., 2019).

II. Trans-metallation step

In this step, the transfer of the R' group from the boron to the Palladium center takes place. Here, R' group changes its center from Boron to Palladium. Thus, this step is called transmetallation, which means ligand transfer from one metallic center to another one (Mehran Farhang et .al, 2022) .

III. The Reductive elimination steps

Reductive elimination: In this step, the coupled product (R-R') is formed and a catalytically active Pd [0]-complex is generated. Here, the oxidation state of Pd changes from Pd [II] to Pd [0], and the target product is eliminated simultaneously (Ahmed et al., 2023).

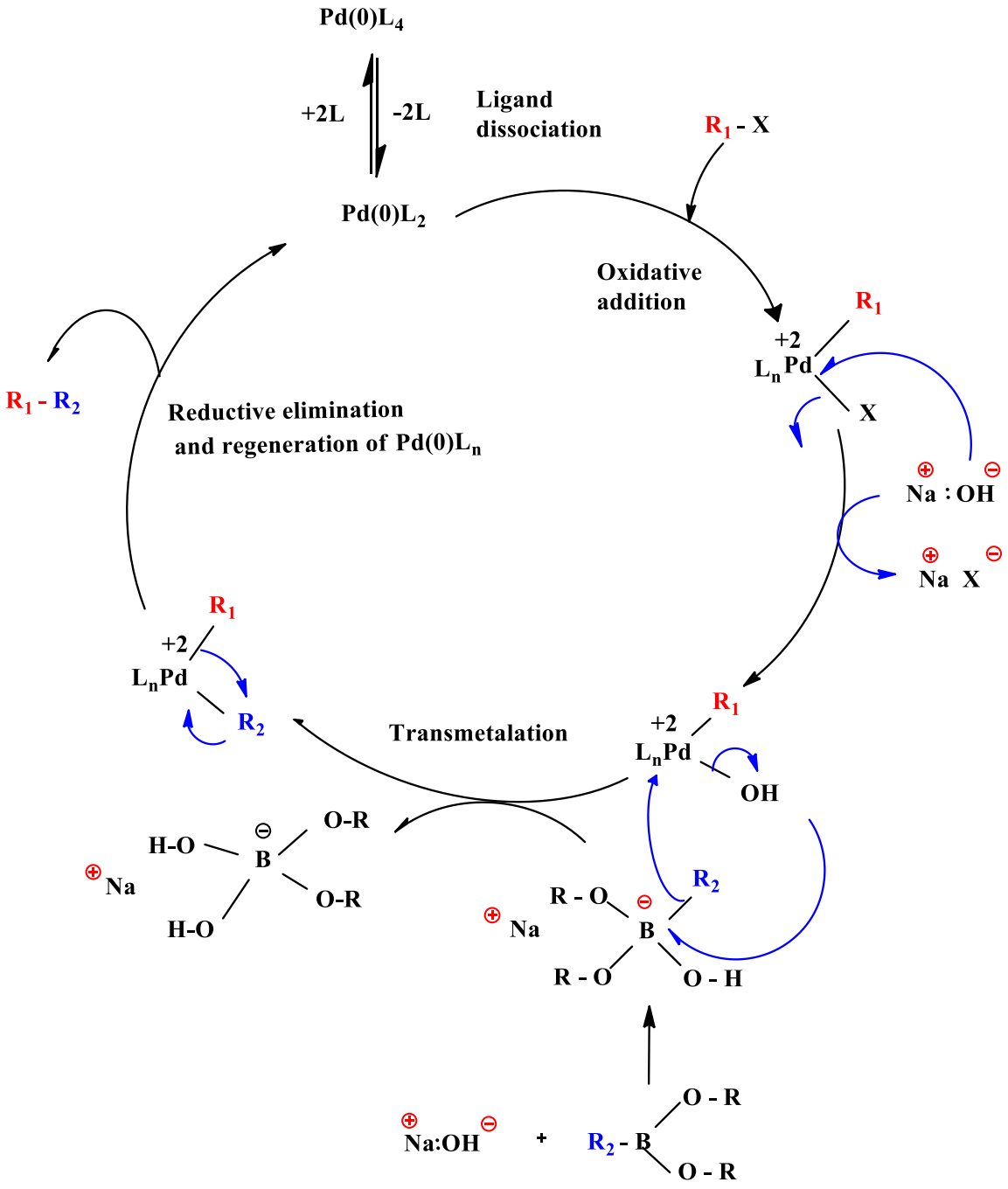

Figure 18 General catalytic cycle for Suzuki cross coupling reaction.

2.13. Knoevenagel Condensation

A Knoevenagel reaction is a condensation between an aldehyde or a ketone and a nucleophilic addition of an active hydrogen compound in the presence of a basic catalyst (ammonia or another amine as catalysts) in organic solvents to yield α, β-unsaturated compounds (Suzaimi Johari, 2022).

Usually, the catalyst is a weakly basic amine, and the active hydrogen compound bears electron-withdrawing groups, such as CO_2R, COR, CHO, CN, or NO_2.

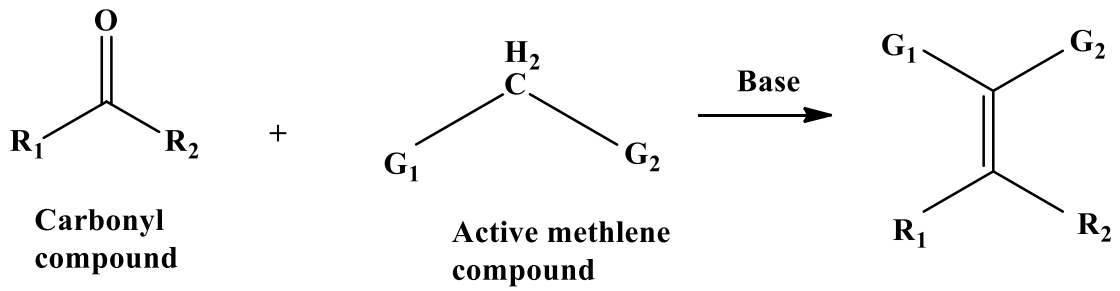

G_1, G_2 = NO_2 , CN, COOR, COOH, SO_2R ,COR, Ar
R_1, R_2 = H, ALKYI

Figure 19 General reaction scheme for the Knoevenagel Condensation.

2.13.1. Mechanism of Knoevenagel Condensation

In the first step of this reaction, an amine base deprotonates the complex methylene (usually a diketone) to form a resonance stabilized anion (enolate). This anion then acts as a nucleophile and attaches to the carbonyl acceptor molecule to form an aldol product, which

can undergo the dehydration reaction to form the α, β-unsaturated product (Wilk et al., 2019).

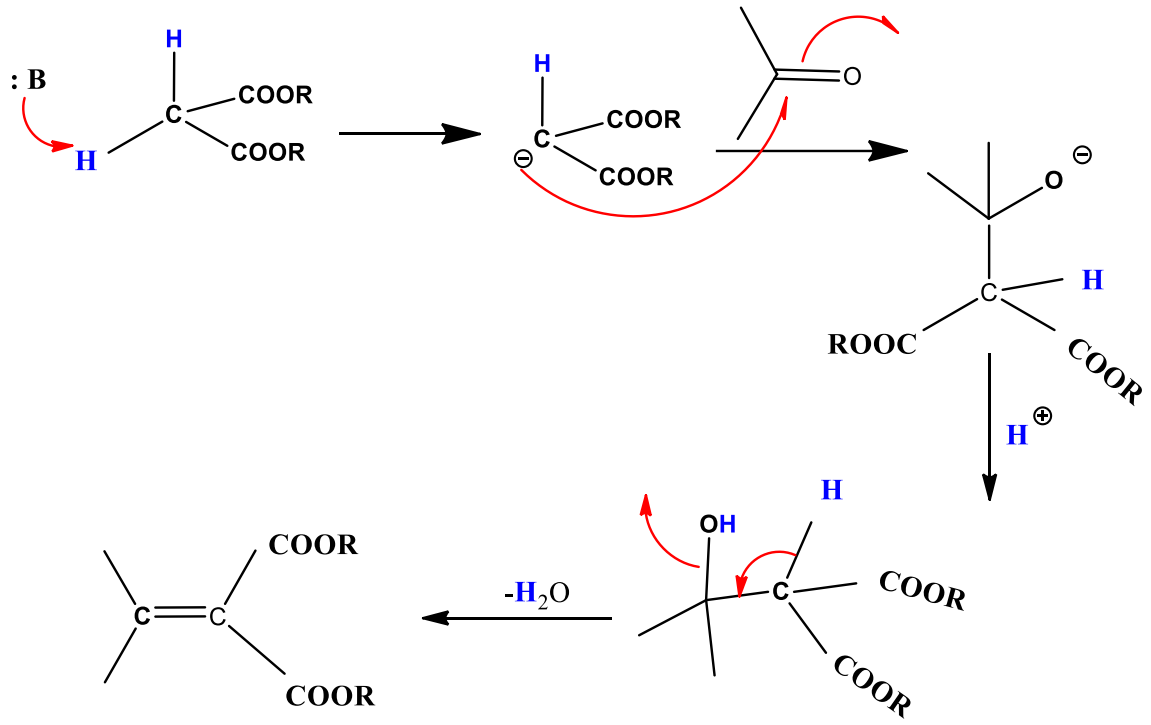

Figure 20 Synthesis of α, β-unsaturated compounds through Knoevenagel condensation

2.14. Comparison between silicon solar cells and DSSCs

Solar energy affords better potential for conversion into electric power (Kamal Prajapat et.al,2023). There are a variety of solar cells available; silicon solar cells are the most common type. The photovoltaic (PV) industry has employed silicon-based solar cells due to the abundance of silicon material and the improved fabrication process (Karim et al., 2019). Among the thin film solar cells, a low-cost solar cell is the dye-sensitized solar cell (DSSCs). Since DSSCs are not dependent on the p-n junction, they differ fundamentally from silicon solar cells. Novel materials, such as nanomaterials, are used to create DSSCs.

Its framework is a semiconductor created by sandwiching an electrolyte and a photo-sensitized anode with an electrochemistry system (Ikpesu et al., 2020).

The advantages of DSSC's are the following:

a) low production cost, Cheap materials are used to manufacture this solar cell, have good shelf life and does not degrade under sunlight.
b) The solar cell works effectively in cloudy climatic conditions and can work at wider angles.
c) It is easy to use, clean, and maintain.
d) These solar cells are composed of lightweight and durable materials and has high mechanical strength.
e) This solar cell can work at wider angles.

The Disadvantages of DSSC's solar cells are the following:

a. DSSC's technology uses liquid electrolyte that has temperature stability problem
b. The electrolyte consists of volatile organic solvents. Thus, it must be sealed with caution. Due to its volatile nature, the dye sensitized solar cell must be installed with precaution.
c. It has less efficiency than other solar cells.
d. These solar cells are not ideal for large-scale applications as more efficient solar panels are required for large-scale deployments.

Disadvantages of traditional silicon are the following:

a. Growing and sawing of ingots is a highly energy intensive process.
b. Requires expensive manufacturing technologies.
c. Fairly easy for an electron generated in another molecule to hit a hole left behind in a previous photo excitation.
d. Much of the energy of higher energy photons, at the blue and violet end of the spectrum, is wasted as heat.

CHAPTER THREE

3.MATERIALS AND METHODS

3.1. General

A major component of this research photovoltaic involves the development of materials to improve solar cell efficiencies and to search for reasonably priced alternatives to the current photovoltaic materials. This thesis also investigates metal free organic small molecules for use in Dye sensitized solar cells. All starting materials were purchased from commercial suppliers (Sigma-Aldrich, Fisherman) and used directly without further processing. The two synthesized reactions were carried out under nitrogen atmosphere in oven-dried flask. THF was dried under nitrogen atmosphere.

Bis (triphenylphosphine) palladium chloride (Pd $(PPh_3)_2Cl_2$) was used as a catalyst to conduct Suzuki coupling reaction processes in THF. The progress of reactions was monitored by thin layer chromatography (TLC) over 0.25 mm pre-coated silica gel plates. Column chromatography was carried out, with silica gel as the stationary phase and various types of solvents as the eluents. Merck 0.25 mm silica gel 60 F254 pre-coated plates on aluminum were used to monitor the progress of reactions by thin layer chromatographic experiments. At 254 and 365 nm, spots were seen using an ultraviolet lamp.

The sensitizers prepared in the course of the synthesized Suzuki Marilyne coupling reaction and Knoevenagel condensation reaction work were purified and characterized by NMR, FTIR, UV-Vis's techniques and both metal free organic small molecules were characterized by photovoltaic performance measurement.

3.2. Reagent

The following chemicals were used: Pd $(PPh_3)_2Cl_2$, EtoAc, Brine, Methanol, Amoniumacetate, THF, Cyanoaceticacid, 2M HCL ,4-bromobenzaldehyde, Na_2CO_3, DCM 4-bromobenzoicacid, Triphenylamine boronic acid, chloroform, CH_3CN, $MgSO_4$, Trimethylsilyl chloride, Ti-Nanoxide T/SP, Ti-Nanoxide R/SP, iodide/tri-iodide (I^-/I_3). Petroleum sprit (40-60 ^oC), CH_2Cl_2 were purchased from BDH and were used as received.

3.3. Synthetic procedures

Two triphenylamine-based dyes (FG_1 and FG_2) were synthesized using similar methods of the Suzuki coupling reaction between different brominated aryl substrates and triphenylamine boronic acid. Degassed the solvent mixture and Reflex laboratory setups for FG_1 and FG_2 are shown below.

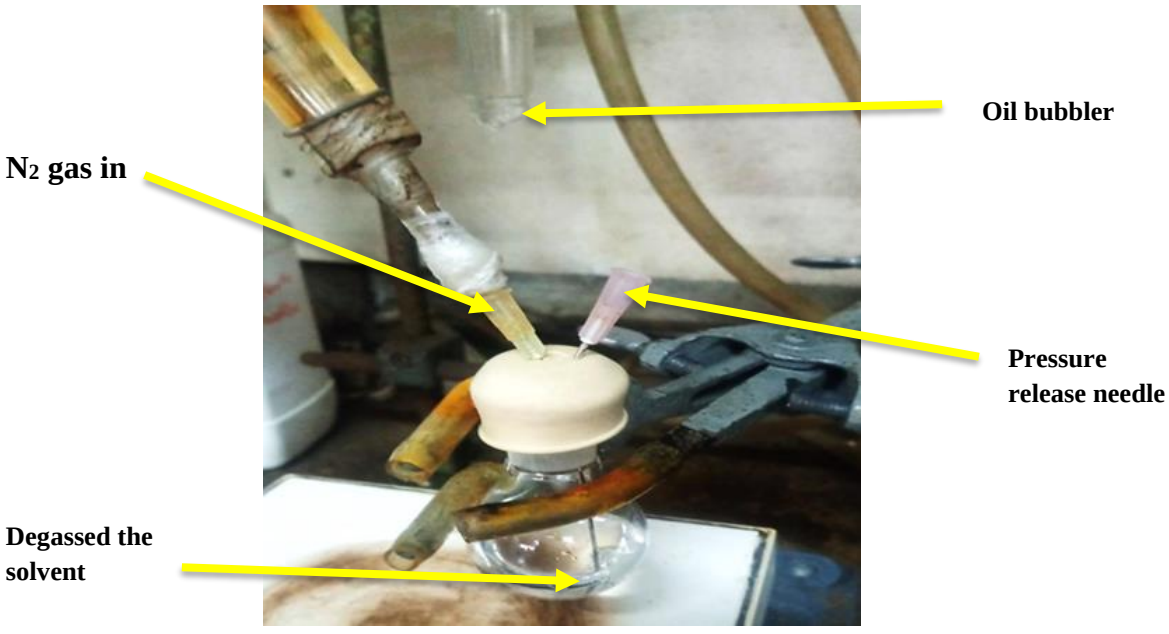

Figure 21 Degassed the solvent mixture for the synthesis of dye

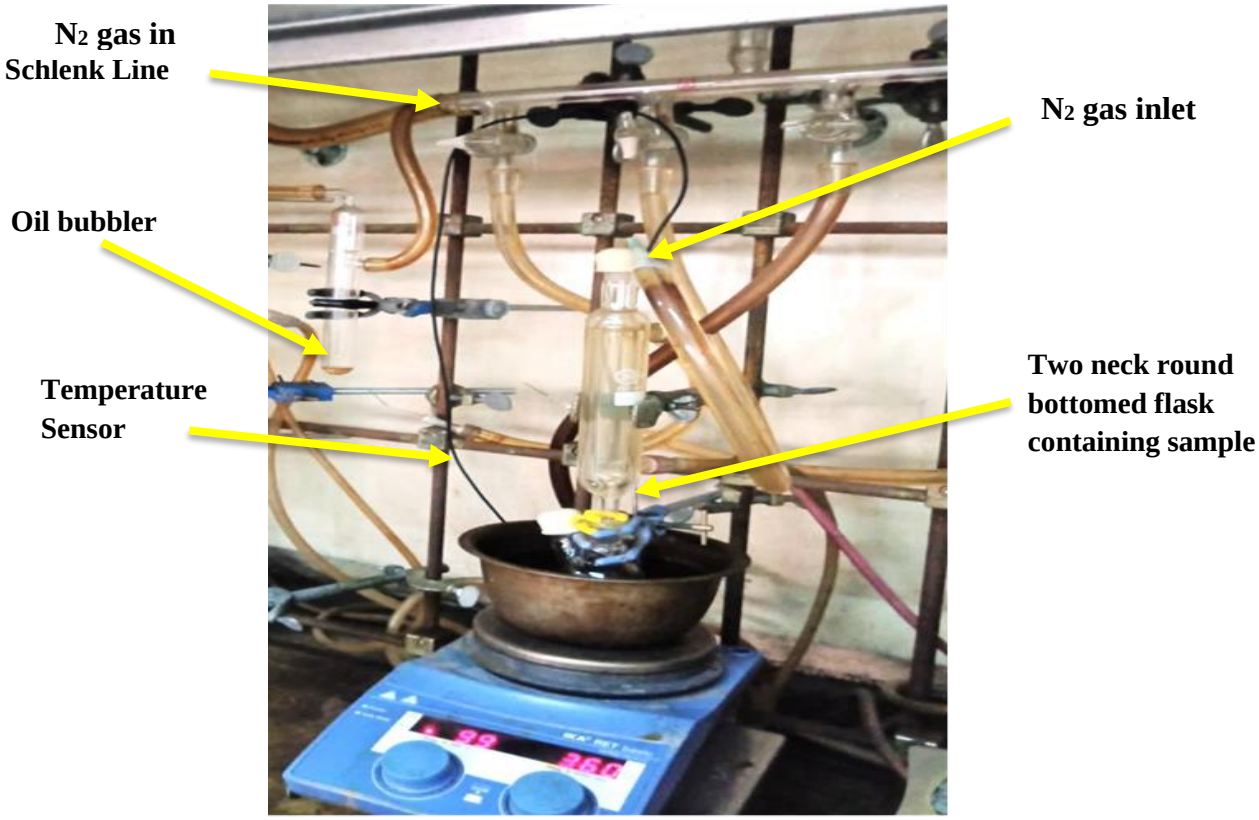

Figure 22 Reflux setup for the Synthesis of organic small molecule dye.

3.3.1. Synthesis of (4-(diphenyl amino) phenyl) boronic acid (FG_1)

4-bromobenzoic acid (0.2211g, 1.1mmol), Triphenylamine boronic acid (0.28914g, 1mmol), Pd $(PPh_3)_2Cl_2$ (0.033g, 0.0466 mmol) and Na_2CO_3 (0.334g, 3.148 mmol) is added to in a 50 ml two-necked round-bottomed flask. Then the reaction mixture adds 20 ml THF/H_20 mixed solvent (v/v = 4/1). The resulting mixture reflux overnight under nitrogen atmosphere with 95^0c. After cooling the solution at room temperature, hydrochloric acid was adding in the reaction mixture and then extracted with CH_2Cl_2. The organic layer is separate and dry over $MgSO_4$ followed by filtration and removal of the solvent by Rota evaporator. The desired product of (FG_1) was obtained as light-yellow fine powder product (0.18 g, 61.9 %) by column chromatography eluted with EA/pet. ether, 1/10.

3.3.2. Synthesis of (E)-2-cyano-3-(4'-(diphenyl amino)- [1, 1'-biphenyl]-4-yl) acrylic acid (FG_2)

Step one: Synthesis of 4'-(diphenyl amino)- [1, 1'-biphenyl]-4-carbaldehyde

4-bromobenzaldehyde (0.204 g, 1.1mmol), Triphenylamine boronic acid (0.28914g, 1mmol), Pd $(PPh_3)_2Cl_2$ (0.033 g, 0.0466 mmol) and Na_2CO_3 (0.334 g, 3.148 mmol) is added to in a 50 ml two-necked round-bottomed flask. Then the reaction mixture adds 20 ml THF/H_20 mixed solvent (v/v = 4/1). The resulting mixture reflux overnight under nitrogen atmosphere with 95^0c. After cooling the solution at room temperature, hydrochloric acid was adding in the reaction mixture and then extracted with CH_2Cl_2. The extract was dried with anhydrous $MgSO_4$ and concentrated by rotary evaporation. The residue was purified by column chromatography (eluent: EA/petroleum ether =1/10). Recrystallization from ethanol: dichloromethane (3:1) obtain the yellow powder (0.25 g, 68.7%).

Step two: Synthesis of (E)-2-cyano-3-(4'-(diphenyl amino)- [1, 1'-biphenyl]-4-yl) acrylic acid (FG_2)

A CH_3CN (20 mL) solution of compound one (0.1487g, 0.5145 mmol) and cyanoacetic acid (0.5145g, 6.05 mmol) was refluxed in the presence of ammonium acetate for 8 h. After removing the solvent, the residue was purified by column chromatography using silica gel and DCM: CH_3OH (v: v, 10:1) mixed as the eluent to give the dye FG_2 as dark red solid (0.170 g, 75.3%).

3.4. Dye Characterization Instrument

3.4.1. UV-Vis's Spectrophotometer

UV-VIS spectrometry concerns the measurement of the on sequences of the interaction of electromagnetic radiation in the UV -visible region with absorbing species like atoms, molecules, or ions. The absorption of ultraviolet or visible light by a molecule will occur when the energy of the incident radiation is the same as that of a possible electronic transition in the molecules involved, as defined (Ammar & , Hemdan S. H. Mohamed et.al , 2019).

This type of energy absorption is known as electronic excitation, and that corresponds to a fraction of an electron from the ground state. The ultraviolet-visible zone of electromagnetic energy ranges from around 200 nm to 800 nm. The Lambert-Beer law expresses the relationship between light absorption, light path (cell thickness), and concentration.

$$A = \log 1/T = \log I / I_O = \epsilon C L \ldots\ldots\ldots\ldots (7)$$

Where: A (Absorbance), T (Transmittance ($T= I / I_O$), the fraction of light transmitted),

$\in$ (Molar absorptivity (molar extinction coefficient)), C (concentration)

L Cell thickness

UV-vis absorption spectra were measured with Perkin-Elmer Lambda 950 and Agilent Technologies Cary 60 UV-Vis's absorption spectrometers as shown in the figure below. The absorption spectra of the two-metal free organics molecules dye were recorded from 300 nm to 800 nm wavelength range and using chloroform solutions of each small molecule.

Figure 23 Perkin-Elmer Lambda - 950 UV- Vis Spectrophotometer

3.4.2. NMR spectroscopy

NMR spectroscopy is a technique based on the absorption of electron magnetic radiation in the radio frequency range of 4 to 900MHz by atom nuclei. ^{1}H NMR and ^{13}C NMR spectroscopy is highly efficient tools for determining the quantity of hydrogen or proton in a compound in addition to information on the carbon backbone of the product's chemical structure. ^{1}H NMR and ^{13}C NMR spectra were recorded on a Bruker Avance 400 spectrometer at 400.13 and 100.06 MHz as shown in the figure below, respectively, with $CDCl_3$ as solvents.

^{1}H and ^{13}C chemical shifts (δ) were reported in ppm downfield from tetramethyl silane (TMS) reference using the residual protonated solvent resonance as an internal standard. The coupling constants are reported in hertz (Hz) and splitting patterns are represented as s (singlet), d (doublet), t (triplet), quin (quintet), sept (septet) m (multiplet) or dd (doublet of doublets).

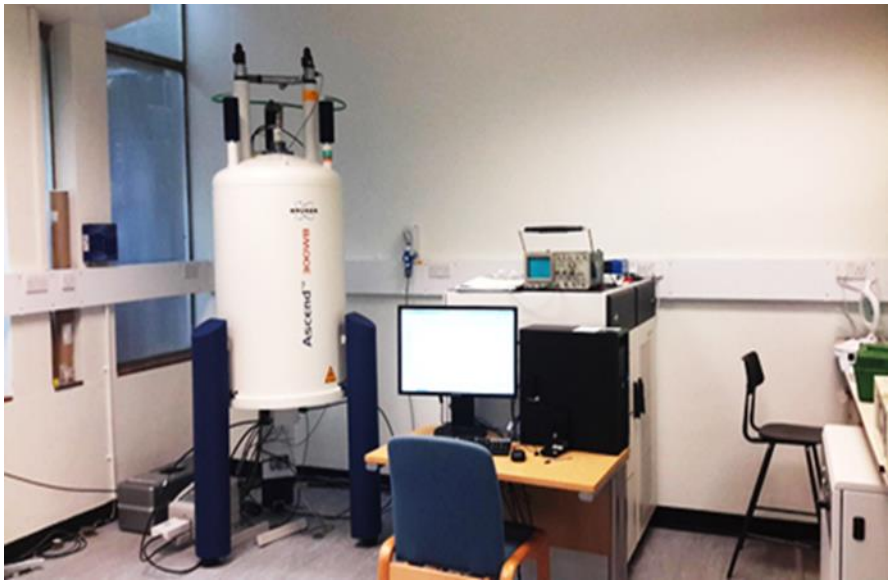

Figure 24 Bruker Avance 400 ^{1}H NMR and ^{13}C NMR spectrometer

3.4.3. Fourier transform infrared (FTIR) Spectrophotometer

Infrared spectroscopy is measured by the interaction of matter with infrared radiation by absorption, emission, or reflection. One of the most effective methods for characterizing new materials, identifying unknown samples, and confirming the existence of known functional groups such as C=O, C-H, or N-H in materials (gas, liquid, and solid) is infrared spectroscopy, which uses an infrared radiation beam. On the electromagnetic radiation spectrum, infrared radiation is located in between microwave and visible radiation.

The infrared region of the electromagnetic spectrum is commonly divided into three subregions namely near-infrared (14000 – 4000 cm^{-1}), mid-infrared (4000 – 400 cm^{-1}), and far-infrared (400 – 40 cm^{-1}).

A common laboratory instrument using this technique is the Fourier transform infrared (FTIR) spectrometer as shown figure below. The major applications are done in the mid-infrared region, between (4000 and 400) cm-^{1}. Each molecule's absorption of infrared radiation was measured using infrared spectroscopy, giving a spectrum that is generally expressed as wavenumber (cm^{-1}) in the x axis versus as percentage of transmittance in the y axis.

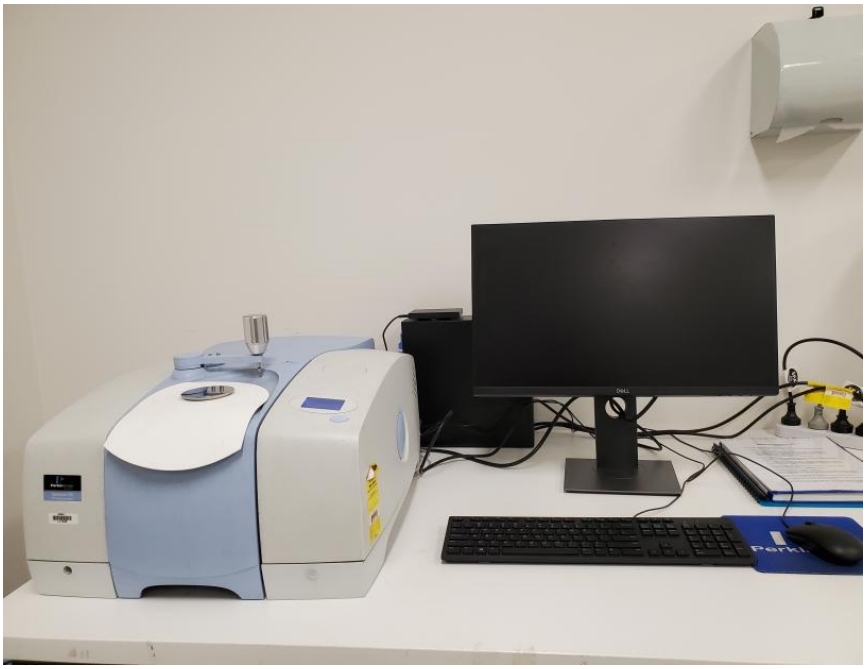

Figure 25 Perkin-Elmer Spectrum 65 FTIR Spectrophotometer

3.4.4. The photovoltaic Measurement

The solar energy conversion efficiency was tested under in lab settings to measure the relationship between current and voltage (I-V) characterization curve been obtain using modified computerization digital Keithley 2400 multimeters under illumination of 100W xelone lamp.

A solar simulator, Power Supply of Solar simulator, Source meter, PC, and Silicon detector is among the tools that are necessary for studying solar cells as show in the figure 25.

(1) Solar Simulator: - is an artificial light source which can generate or simulator the natural sunlight with similar spectral distribution and light intensity.

(2) PC: - to process the data, user uses usually a personal computer. And to connect PC with measurement equipment, some interfaces are needed. operating the keithley source meter required using a pc operating the lab view software.

(3) Source meter: - is measuring equipment current and voltage, which can apply bias voltage during measurements. The keithley model 2400 high current source meter instrument to measure the current-voltage (I-V) characteristics of photovoltaic cells.

Figure 26 AM1.5 Oriel solar simulator and Keithley 2400 source meter set-up for PCE measurements

(4) Power Supply of Solar simulator: - Conventional solar simulators have long relied on xenon arc lamp technology to match the solar spectrum as show in the figure below.

(5) Silicon detector/Illumination meter or Irradiance meter is very important to adjust solar simulator irradiance for measuring and calculating I-V curves and efficiencies as shown below.

Figure 27 Power supply and Irradiance meter for Keithley 2400 source meter

3.5. Preparation of dye sensitized solar cell (DSSCs)

3.5.1. Preparation of photoanode electrode

The fabrication procedures of the patterned DSSCs can be seen below, with different steps. The glass plates with Fluorine -doped tin oxide (FTO) 10 cm x10 cm were first cut into 1.5 cm by 2.5 cm square pieces using a diamond tip as shown Figure 28, and the two slides for one cell.

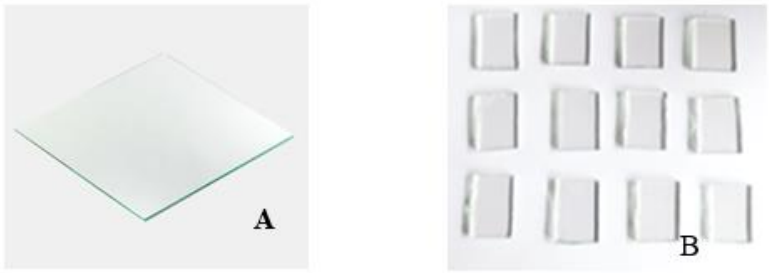

Figure 28 (A) 10cm*10cm (FTO) Florine doped tin oxide glass and (B) FTO glass resized.

The piece of FTO-coated glass substrates was washed by using VWR ultrasonic bath is cleaning applied a liquid soap with water for 15 minutes. After that, the distilled water is sonicated twice for 15 minutes each, and the conductive glass is then sonicated with solvents (ethanol and acetone) in a 1:1 ratio for an additional 15 minutes as shown figure 28. This cleaning process serves to remove any dust particles or contaminating organic matter (e.g., fingermarks) from the FTO surface.

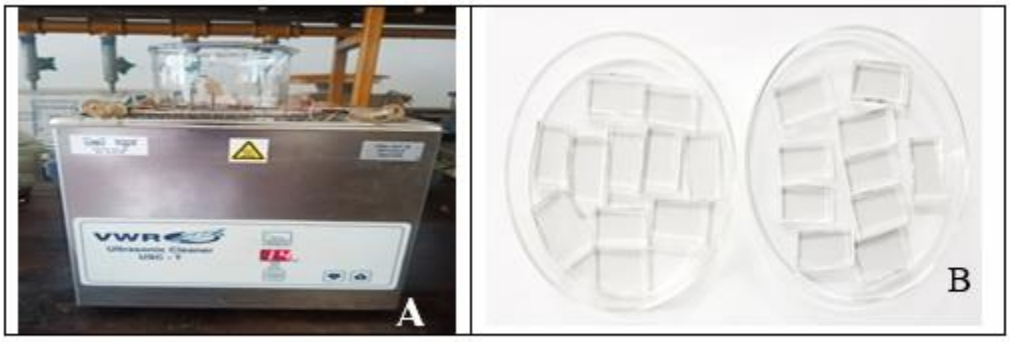

Figure 29 (A) Cleaning process using VWR ultrasonic cleaner and (B) cleaned glass

The substrates were handled using metal tweezers. The correct area to position the tweezers so as to avoid touching the active area of the device. The cleaned glass substrates were dried in the oven for an hour at 120°C. The conducting side of the FTO glass is placed upside down, identified with a voltmeter as shown figure below.

Figure 30 (A) Measuring resistivity and (B) Dried cleaned glass in the oven

First, the conducting sides of the FTO glass are tapped down with Scotch tape. In this experiment, two types of TiO_2 paste were used. Using the doctor's blade technique, a transparent coating of Ti-Nanoxide (T/SP) paste was applied uniformly on FTO-coated glass along a working area.

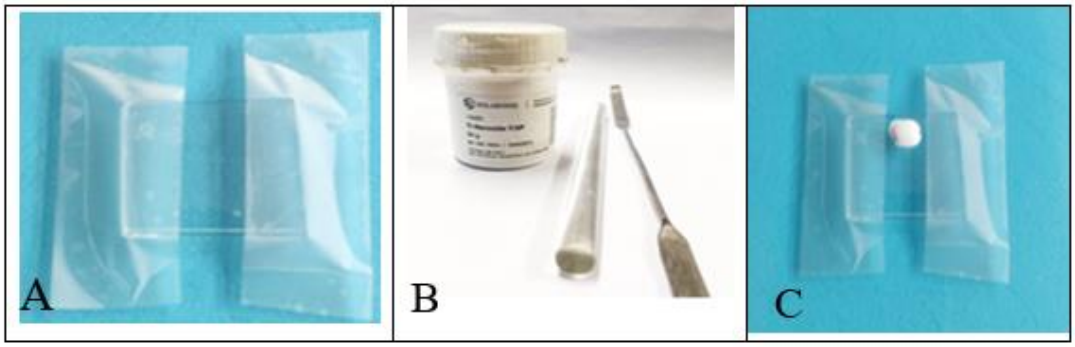

Figure 31 (A) Scotch tape is applied to define the deposition area (B) Transparent TiO_2 paste with rolling glass rode for using doctor blade technique (C) Putting few drops of paste

The coated FTO glass was then allowed to dry at room temperature for an hour to keep the fluidity of the TiO_2 paste and to complete removing the moisture. Oven dried for 45 minutes at 120°C.The coated FTO glass turned a light brown color.

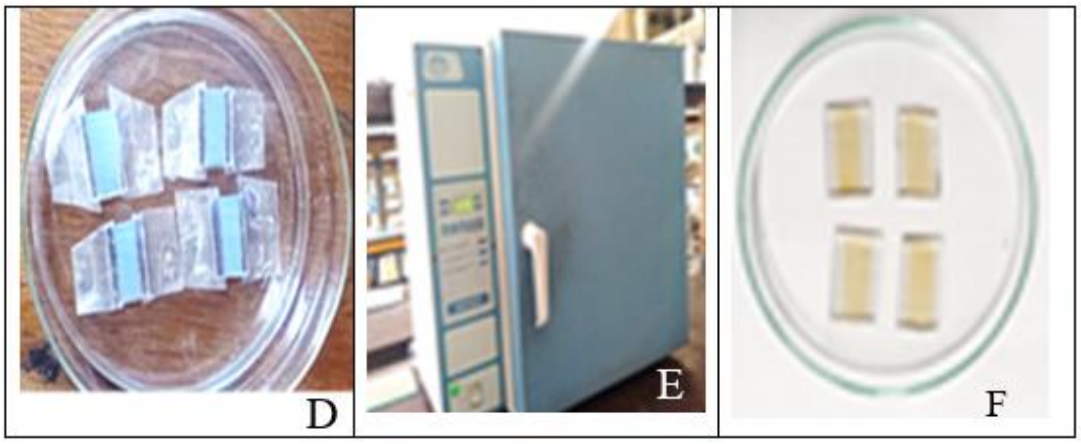

Figure 32 (D) The coted FTO dried at room temperature (E) Further drying by Oven at 120^0C for 45 minutes (F) Dried FTO glass

The samples were annealed in a muffled furnace at 120 °C for 10 minutes, 325 °C for 15 minutes, 375 °C for 15 minutes, and 450 °C for 30 minutes. After the sintering procedure was completed, the TiO_2-coated electrode was cooled overnight inside the furnace to avoid cracking the glass

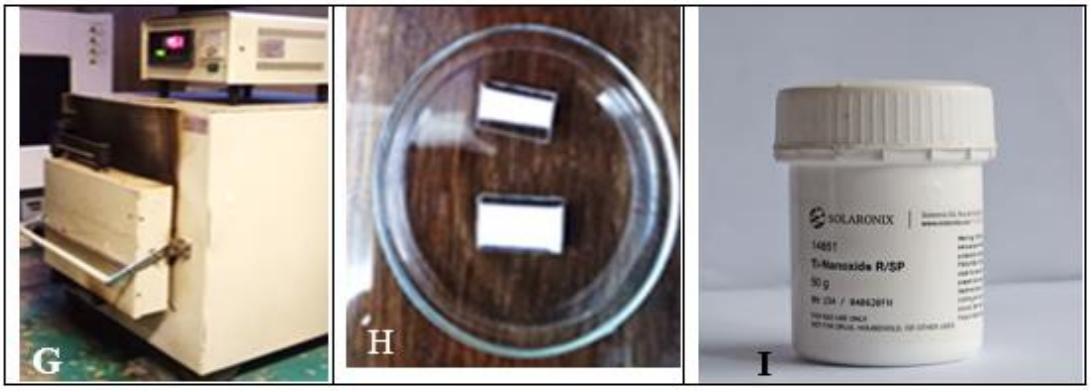

Figure 33(G) Annealed Muffle Furness with growing temperature (H) The sintered TiO_2 cooled at room temperature (I) Ti-Nano oxide R/SP add-on layer

Second, the compact TiO_2 layer was covered with a refractive TiO_2 paste (Ti -Nanoxide R/SP), which was sintered under the same circumstances.

Figure 34 Applied Ti-Nano oxide R/SP on sintered transparent TiO_2 active layer (K) muffle Furness (L) sintered FTO glass with refractive active layer (M) Resizing the working area (0.5*0.5 cm) FTO glass

3.5.2. Preparation of the counter electrodes

The counter electrode glass formed using the same technique as the photo-anode. The conducting side of the FTO glass was fabricated by covering a partially conductive surface with graphite (HB/8HB pencil).

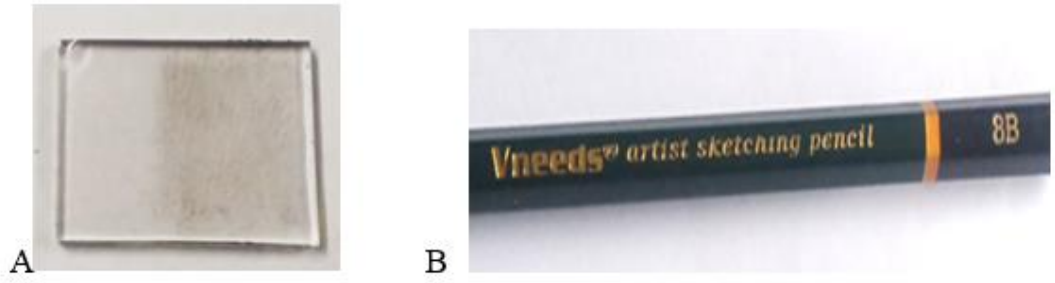

Figure 35 (A) Coat the FTO glass substrate with by graphite (B Graphite pencil

According to (Wu et al. 2017, and Gullace et al., 2020), carbon materials are the most promising material for the counter electrode in DSSCs and the best alternative to platinum electrodes (Wu et al. 2017; Wu and Ma 2012). Counter electrodes are used to regenerate the electrolyte, with the oxidized electrolyte diffusing towards the counter electrode.

3.5.3. Preparing a dye solution and socked Photo-anode

About 0.03 mg of the two dye powders should be dissolved in 25 mL of acetone while being stirred until no trace of solid remains. The dye molecules are adsorbed to the TiO_2 particles after the dipping process, and the TiO_2 film is said to be "sensitized" to the dye molecules.

Figure 36 Dip the TiO2 electrode into the dye solution.

The backside of the film shows dark coloring as the outcome of the dye molecules settling in particular area locations in the mesoporous TiO_2 layer. The top side of the film little changes color since there are not many dye molecules adsorbed in the scattering layer. After removing the electrode from the bath, carefully ethanol-rinse the stained titania.

3.5.4. Assembly of DSSCs

As shown in the figure, the sensitized electrode and graphite-coated counter electrode had been held using binder clips and were facing each other from the conducting side. A small quantity of electrolytes was seeped into the cell to allow charge transportation between the electrodes.

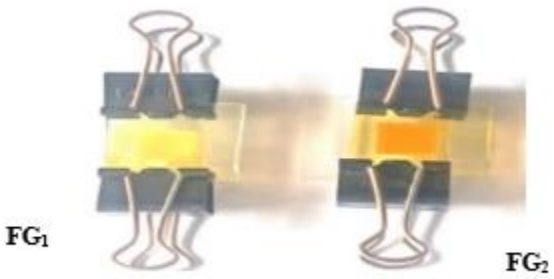

Figure 37 Assembled device of FG_1 and FG_2 dyes.

CHAPTER FOUR

4. RESULTS AND DISCUSSION

To study metal free organic small molecules and fabricate dye-sensitized solar cells, experimental and computational methods were used in this research. The structural features of the compounds 4'-(diphenylamino)- [1, 1'-biphenyl]-4-carboxylic acid (FG_1) and (E)-2-cyano-3-(4'-(diphenylamino)- [1, 1'-biphenyl]-4-yl acrylic acid (FG_2) were confirmed their structure of the symmetrical compounds by UV-vis absorption, ^{1}H and ^{13}C-NMR and FTIR spectra. The metal free organic dye exhibit good solubility in organic solvents like methanol, chloroform, and THF at room temperature.

Synthesis and structural characterization

Synthesis of (4'-(diphenylamino)- [1, 1'-biphenyl]-4-carboxylic acid) (FG_1)

The Suzuki reaction performed using a palladium catalyst to couple Triphenylamine boronic acid and 4-bromobenzoic acid. Compound (FG_1) was obtained in 61.9% yield as a light-yellow powder as shown in figure below.

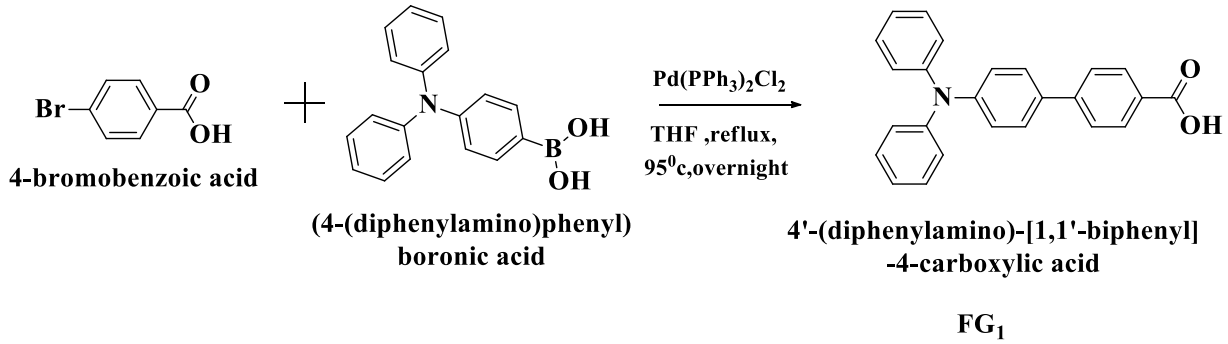

Figure 38 Synthesis of compounds 4'-(diphenylamino)- [1, 1'-biphenyl]-4-carboxylic acid FG_1.

Synthesis of (E)-2-cyano-3-(4'-(diphenylamino)- [1, 1'-biphenyl]-4-yl) acrylic acid (FG_2)

And also, the second compound undergo Suzuki cross-coupling reactions of 4-bromobenzaldehyde with Triphenylamine boronic acid in THF with Pd $(PPh_3)_2Cl_2$ as the catalyst gave 4'-(diphenylamino)- [1, 1'-biphenyl]-4-carbaldehyde. The aldehydes finally undergo knoevenagel condensation with cyanoacetic acid in the presence of ammonium acetate yielded the target dye FG_2. As shown in figure below.

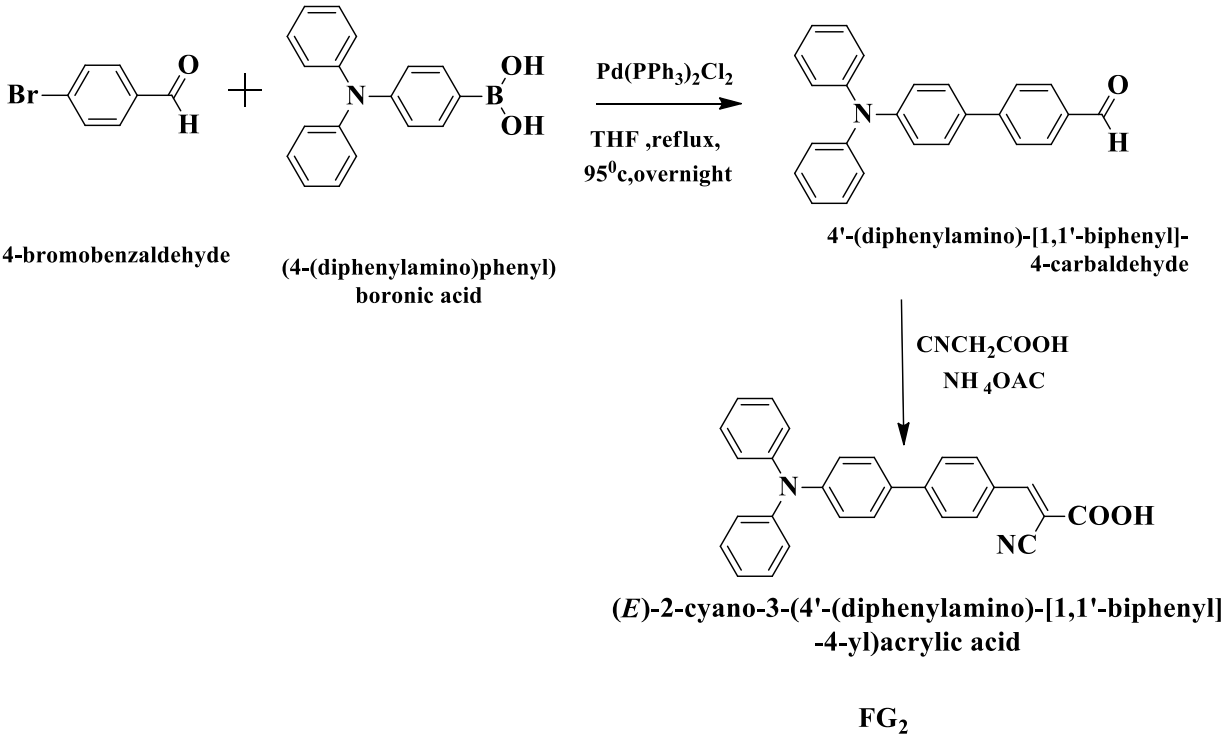

Figure 39 Synthesis of (E)-2-cyano-3-(4'-(diphenylamino)- [1, 1'-biphenyl]-4-yl) acrylic acid (FG_2).

Compound (FG_2) was obtained in 75.3% yield as a dark red solid powder, and the structure of the symmetrical compounds (FG_2) was confirmed with its ^{1}H, ^{13}C-NMR and FTIR spectra.

4.1. UV-vis absorption spectra of the two dyes (FG_1&FG_2)

The UV-vis absorption spectra of 4'-(diphenylamino)-[1,1'-biphenyl]-4-carboxylic acid (FG_1) and (E)-2-cyano-3-(4'-(diphenylamino)-[1,1'-biphenyl]-4-yl) acrylic acid (FG_2) in methanol solutions are displayed in figure below. All dyes exhibited broad absorption spectra ranging from 270 to 525 nm.

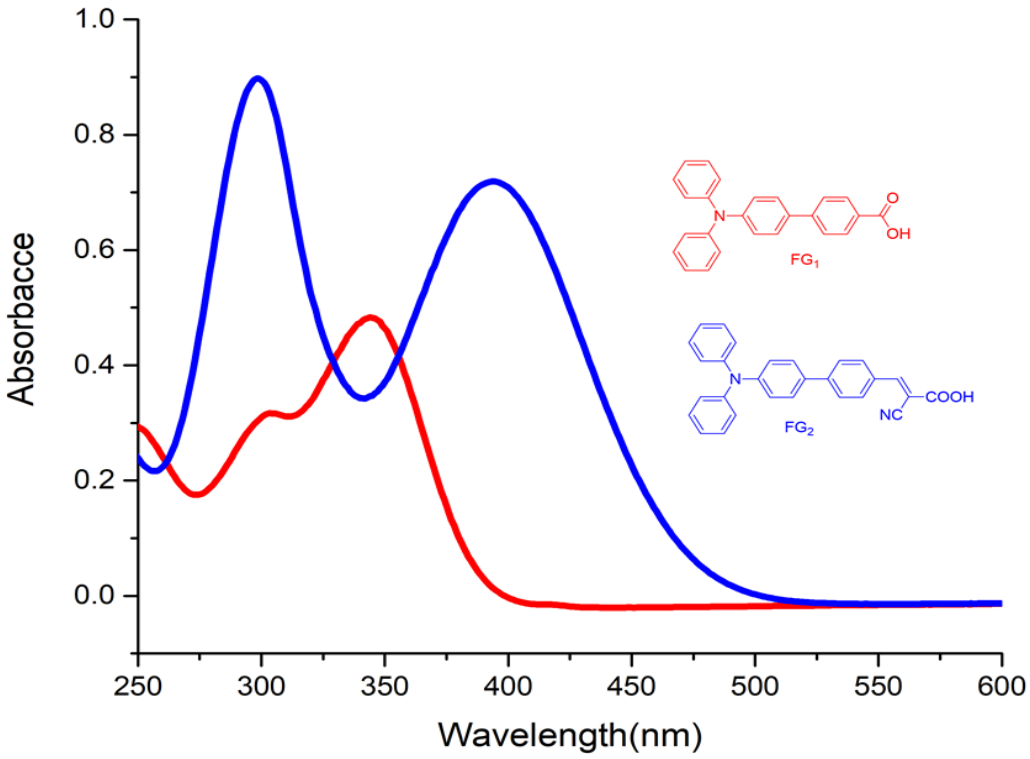

Figure 40 UV-vis absorption spectra of the dyes in methanol solutions

The two different absorption bands placed between 200 and 350 nm correspond to localized aromatic π–π* transitions. The intermolecular charge transfer (ICT) transition is responsible for the absorption bands in the low-energy range of about 400–600 nm transitions between the electron-donating triphenylamine and the electron-accepting cyanoacrylic acid. The highest absorption peaks of dyes FG_1 and FG_2 with carboxylate acid and cyanoacetic acid as anchoring groups were 344 and 425nm, respectively. Furthermore, the presence of double bond and electron with drawing group is responsible the absorption peaks of FG_2 with a cyanoacrylic acid unit as an anchoring group displayed a red shift compared to FG_1 with a carboxylate unit as an anchoring group.

4.2. $^{1}H,^{13}C$-NMR and DEPT spectra of FG_1 and FG_2

4.2.1. FG_1 of NMR spectrum

4.2.1.1. ^{1}H-NMR spectrum of 4'-(diphenylamino)-[1,1'-biphenyl]-4-carboxylic acid (FG_1).

^{1}H NMR (400 MHz, $CDCl_3$) δ 8.18 (d, J = 8.3 Hz, 1H), 7.70 (d, J = 8.5 Hz, 1H), 7.55 (d, J = 8.7 Hz, 1H), 7.36 – 7.26 (m, 3H), 7.21 – 7.14 (m, 3H), 7.13 – 7.05 (m, 1H).

In the ^{1}H-NMR spectrum of compound FG_1 seven proton signals in the aromatic region were observed in the figure 41. The aromatic doublets at δ 8.18, 7.70 and 7.55 corresponding to H-3 & 3', H-4 & 4' and H-7 & 7', respectively. The multiplet at δ 7.36 – 7.26, 7.21 – 7.14, 7.13 – 7.05 are due to H-8 & 8', H-11 & 11' and H-13, respectively.

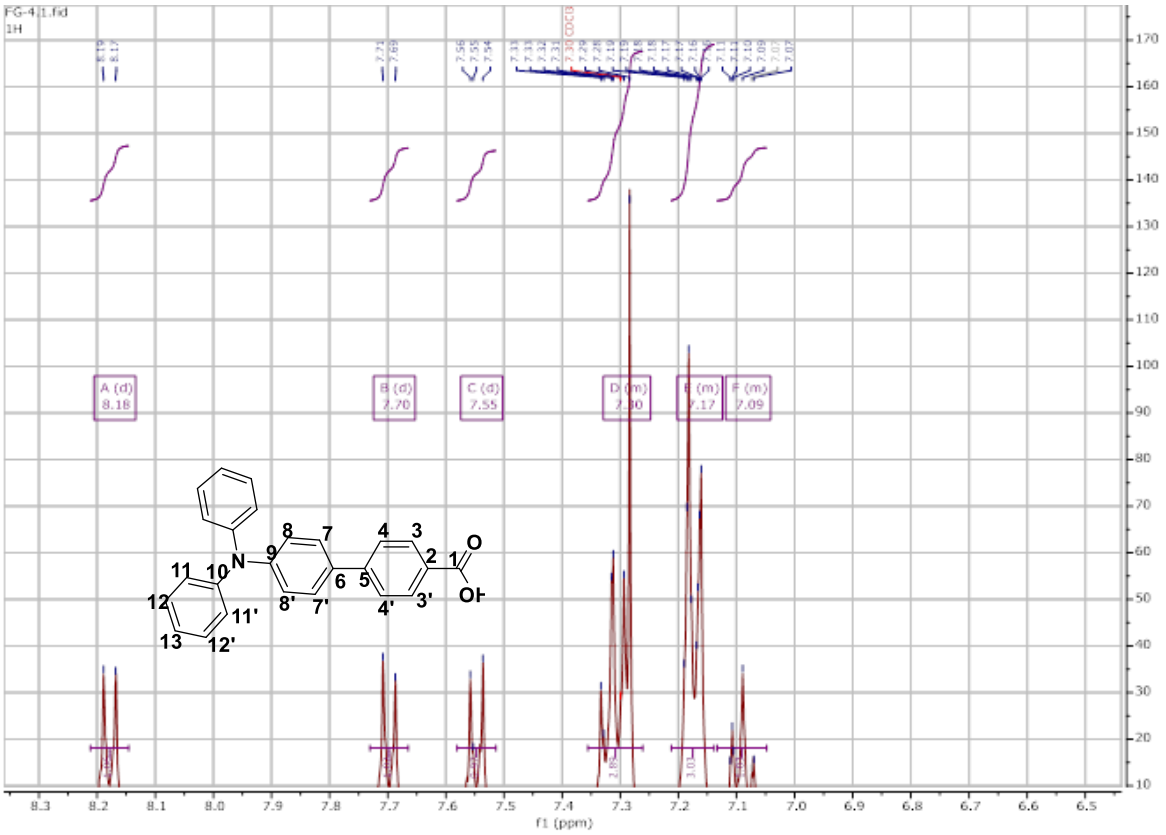

Figure 41 ^{1}H-NMR spectrum of 4'-(diphenylamino)-[1,1'-biphenyl]-4-carboxylic acid (FG_1).

4.2.1.2. ^{13}C NMR of spectrum of 4'-(diphenylamino)-[1,1'-biphenyl]-4 carboxylic acid (FG_1)

^{13}C NMR (101 MHz, $CDCl_3$) δ 148.24, 147.41, 145.91, 133.12, 130.78, 129.39, 127.98, 127.23, 126.45, 124.80, 123.37, 123.27.

The ^{13}C-NMR spectrum showed twelve carbon resonances in the aromatic region as shown in the figure 42. The downfield signal at δ 148.24, 147.41, and 145.91 corresponds to C-9 and C-10 attached to the strong electron-withdrawing nitro-groups while the up-field signal at δ 123.27, 127.98, 127.23, 126.45, 124.80, 123.37, 123.27 is due to C-4 & C-4', C-8 & C-8', C-11& C-11' and C-12 & C-12', C-13.

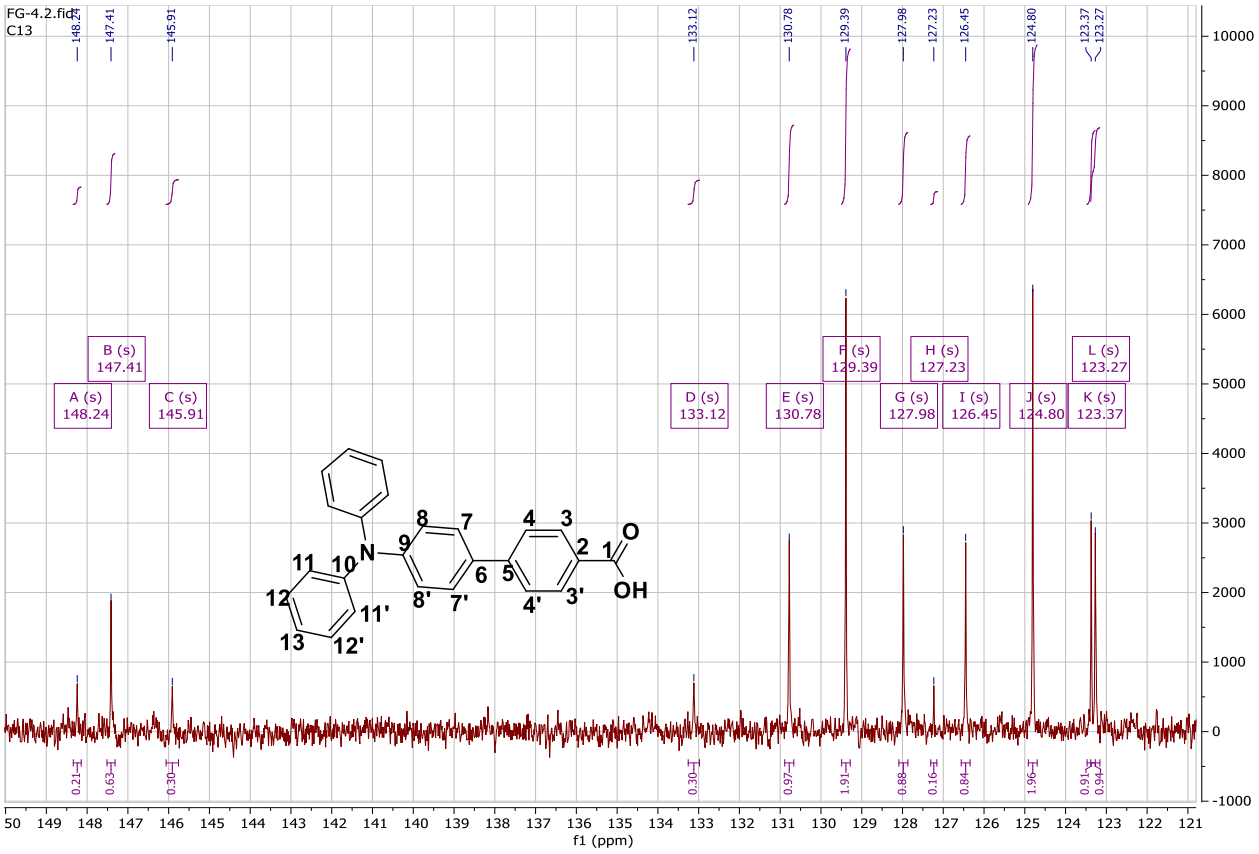

Figure 42 The ^{13}C NMR of spectrum of 4'-(diphenylamino)-[1,1'-biphenyl]-4-carboxylic acid (FG_1).

4.2.1.3. DEPT-135 spectrum of 4'-(diphenylamino)-[1,1'-biphenyl]-4-carboxylic acid (FG_1).

The DEPT-135 spectrum of FG_1 showed seven signals in the aromatic region, corresponding to methylene carbon resonance. The DEPT-135 conforms to molecular symmetry by giving exactly seven spectra as shown in figure 43:

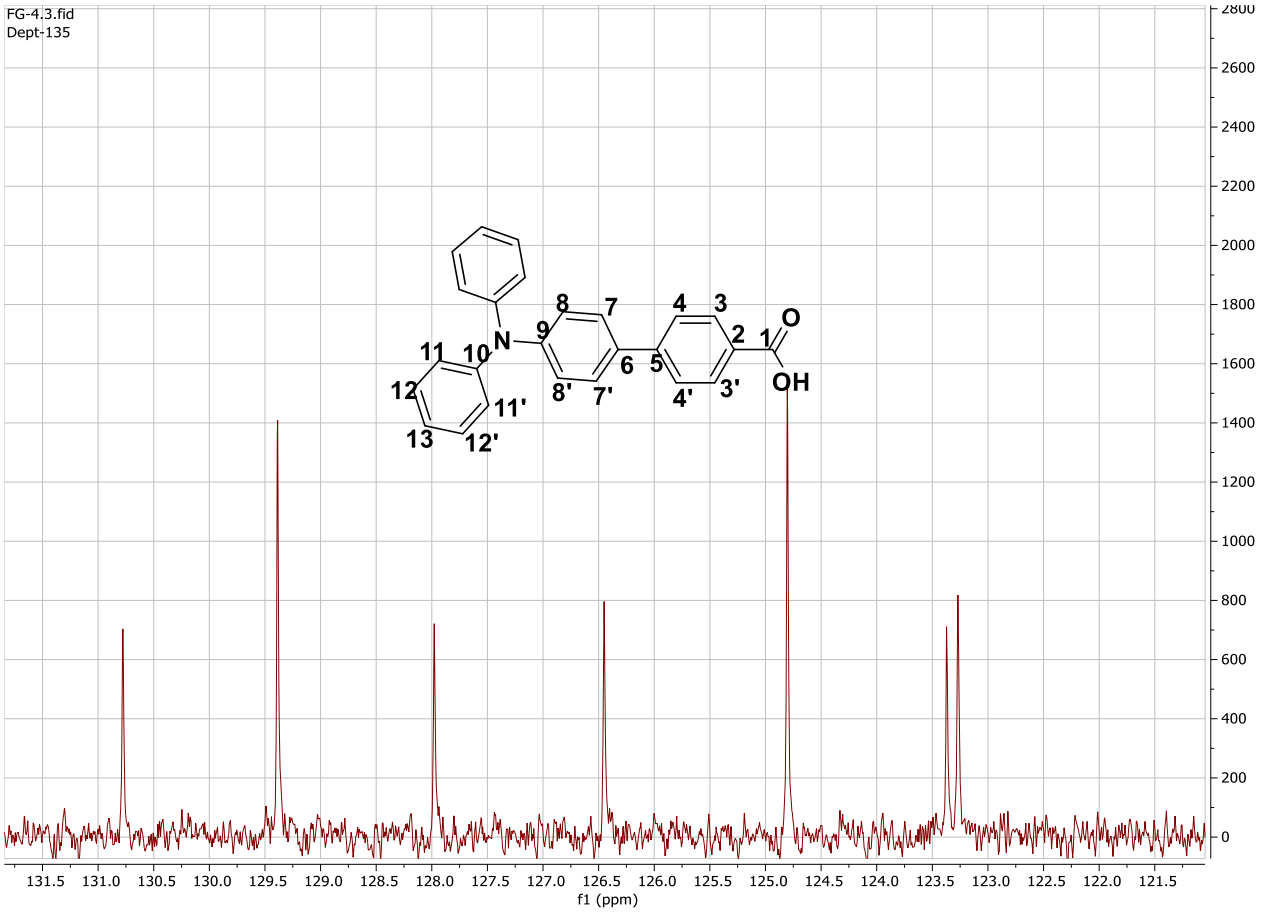

Figure 43 The DEPT – 135 spectra of 4'-(diphenylamino)-[1,1'-biphenyl]-4-carboxylic acid (FG_1).

4.2.2. FG_2 of NMR spectrum

4.2.2.1. ^{1}H-NMR spectrum of FG_2 (E)-2-cyano-3-(4'-(diphenylamino)-[1,1'biphenyl]-4-yl) acrylic acid.

^{1}H NMR (400 MHz, $CDCl_3$) δ 8.35 (s, 1H), 8.12 (d, J = 8.2 Hz, 1H), 7.75 (d, J = 8.4 Hz, 1H), 7.56 (d, J = 8.3 Hz, 1H), 7.36 – 7.26 (m, 3H), 7.18 (d, J = 7.3 Hz, 4H), 7.11 (t, J = 7.3 Hz, 1H) as shown in figure 44.

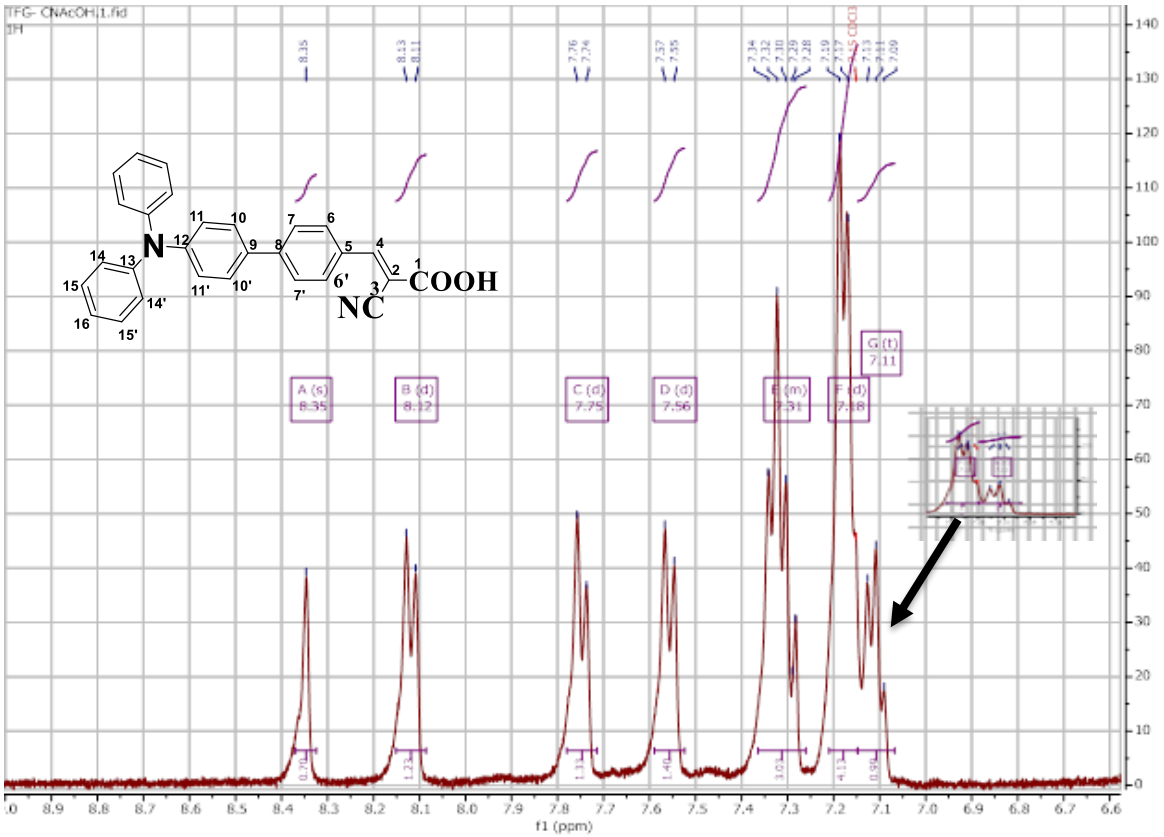

Figure 44 ^{1}H NMR of FG_2 (E)-2-cyano-3-(4'-(diphenylamino)-[1,1'-biphenyl]-4-yl) acrylic acid.

In the ^{1}H-NMR spectrum of compound FG_2 showed seven proton signals in the aromatic region and one signal in the double bond (= CH_2). The one singlet at δ 8.35 (s, 1H) is corresponds to ethylene proton at the H- 4. The three doublets at δ 8.12 (d, 1H), 7.75 (d, 1H) 7.56 (d, 1H) and 7.18 (d, 4H) are due to H-7&7', H-10 &10' and H-11 &11' respectively. The multiplet at 7.36 – 7.26 (m, 3H) is crossponding to H-16. The triplet at 7.11 (t, 1H) is attributed to H-14 &14.

4.2.2.2. ^{13}C NMR of spectrum of 4'-(diphenylamino)-[1,1'-biphenyl]-4 carboxylic acid (FG_2)

^{13}C NMR (101 MHz, $CDCl_3$) δ 167.48, 156.17, 148.73, 147.21, 146.15, 132.31, 132.06, 129.46, 127.94, 127.01, 125.05, 123.67, 122.85, 115.49, 100.54.

The ^{13}C-NMR spectrum of compound FG_2 showed sixteen carbon resonances of which twelve appeared in the aromatic region and the remaining five in the acceptor region. The most downfield signal at δ 167.48 is due to the cyanoacrylic acid carbonyl carbons. The resonances methane carbon at δ 156.17 is attributed to C-4 and H-4 as shown figure 45.

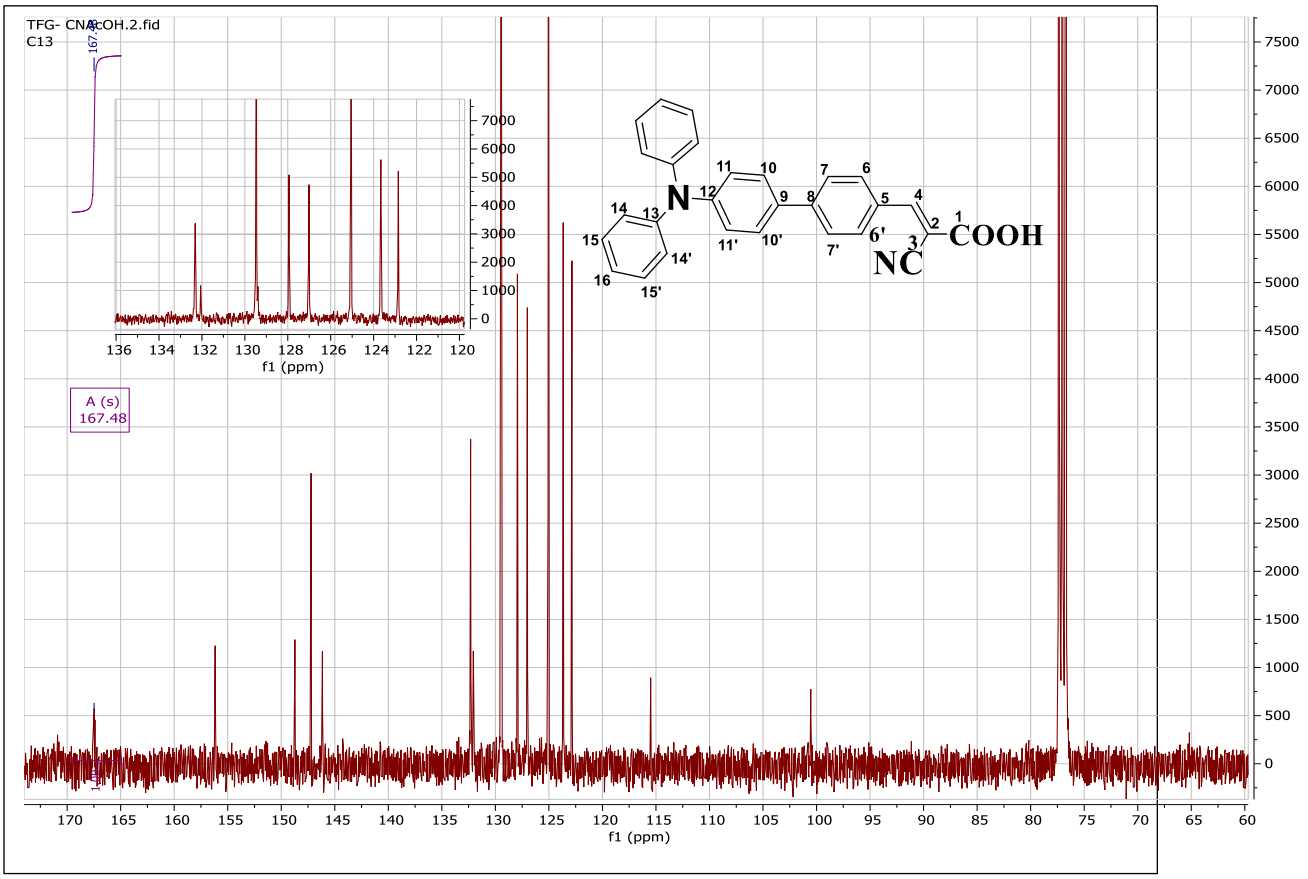

Figure 45 The ^{13}C NMR of spectrum of (E)-2 cyano-3-(4-(4'-(diphenylamino)-[1,1'-biphenyl]-4-yl) acrylic acid

4.2.2.3. DEPT-135 spectrum of (E)-2-cyano-3-(4'-(diphenylamino)-[1,1'-biphenyl]-4-yl) acrylic acid. (FG_2).

The DEPT-135 spectrum of FG_2 showed eight signals in the aromatic region, corresponding to methylene carbon resonance as shown in figure 46.

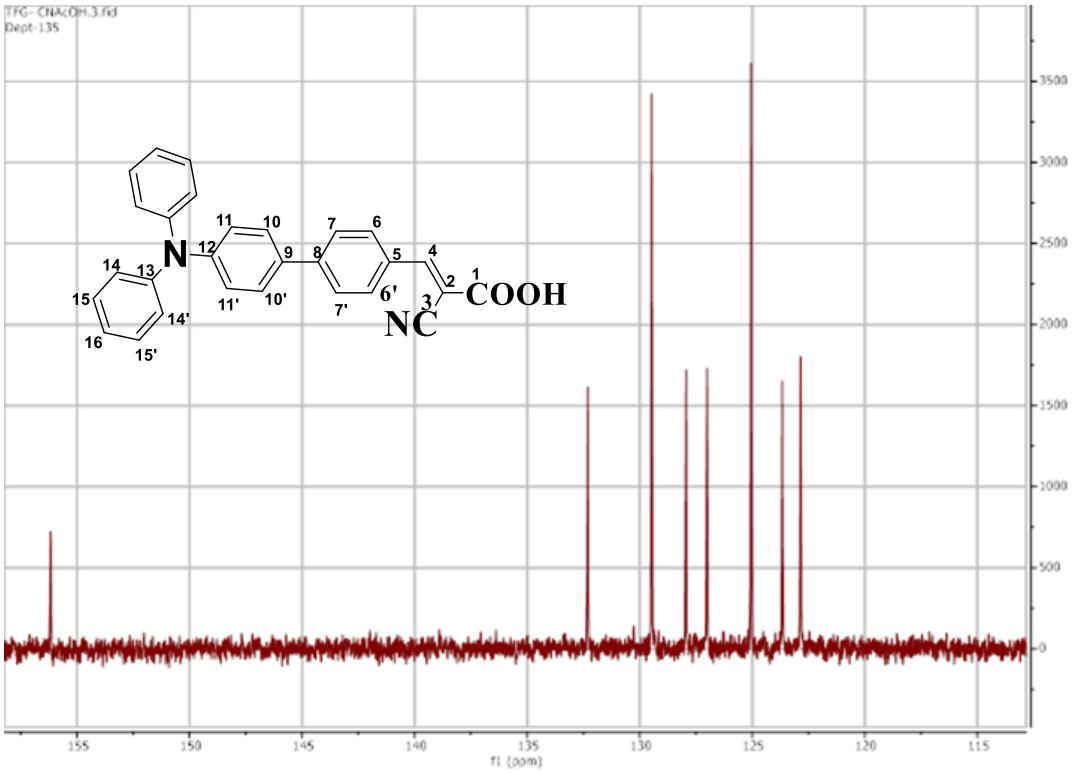

Figure 46 The DEPT-135 spectrum of (E)-2-cyano-3-(4'-(diphenylamino)-[1,1'-biphenyl]-4-yl) acrylic acid (FG_2).

4.3. Fourier Transform Infrared (FTIR) Analysis

FTIR spectra result shows the main peak in absorbance wave numbers spectrum range from 4000 cm^{-1} to 400 cm^{-1} as shown in figure 47. The chemical structure of TPA derivative of synthetic dyes was verified using FTIR investigations.

The appropriate structure of the synthesized FG_1 (4'-(diphenylamino)-[1,1'-biphenyl]-4-carboxylic acid) and FG_2 ((E)-2-cyano-3-(4'-(diphenylamino)-[1,1'-biphenyl]-4-yl) acrylic acid) compounds was confirmed by FTIR spectra.

From the FG_1 compound result obtain shows a peak at 3475 $cm^{-1}$is a vibration typically assigned to hydroxyl groups (OH−), and the absorption bands at 3061, and 3035 cm^{-1} are attributed to aromatic C–H bending vibrations of compound FG_1.The region at 2930 cm^{-1}confirms the presence of C-H asymmetric stretching vibrations in the structure of the sample.

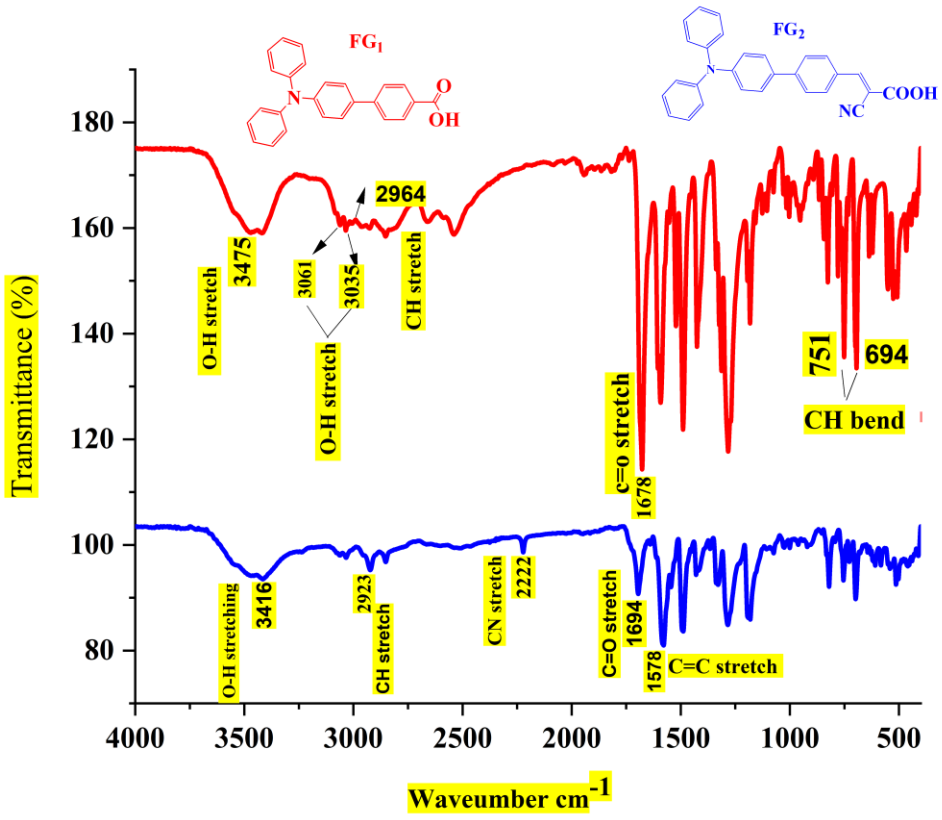

Figure 47 The DEPT-135 spectrum of (E)-2-cyano-3-(4'-(diphenylamino)-[1,1'-biphenyl]-4-yl) acrylic acid (FG_2).

The absorption bands at 1737 cm^{-1} are assigned to the stretching vibration of the carbonyl group and those at 1678 and 1588 cm^{-1} are due to the aromatic C=C groups. The regions 751 and 694 cm^{-1} are assigned to the C-H bend on the aromatic compound. FT-IR spectrum of the FG_1 compound.

The FTIR spectrum of FG_2 molecule shows a broad absorptions band for acidic hydroxyl (O-H) stretching at 3416 cm^{-1} that correspond to vibration of carboxylic group. A strong IR absorption band at 1694 cm^{-1} accounts for C=O stretching, conforming the carbonyl group of carboxylic groups.

Also, the absorption band at 2222 cm^{-1} indicate the presence of the C=N (nitrile) stretching confirming the formation of product [(E)-2-cyano-3-(4'-(diphenylamino)-[1,1'-biphenyl]-4-yl)] acrylic acid (FG_2). The aromatic C=C stretching vibrational band confirmed peak at 1578 cm^{-1}. The peak observed around 750 cm^{-1} corresponds to the aromatic C-H bending vibration.

4.4. Photovoltaic Performance

The photovoltaic performance of the two dyes 4'-(diphenylamino)-[1,1'-biphenyl]-4-carboxylic acid (FG_1) and (E)-2-cyano-3-(4'-(diphenylamino)-[1,1'-biphenyl]-4-yl) acrylic acid (FG2) were measured under the standard global AM 1.5 G irradiation condition and computer integrated Keithley 2400-EC source was used to calculated the photoelectric conversion efficiency of the fabricated DSSCs devices.

Dye FG_1 [4'-(diphenylamino)-[1,1'-biphenyl]-4-carboxylic acid] cell had a short circuit photocurrent density (J_{sc}) of 3.75 $mAcm^{-2}$, an open-circuit voltage (V_{oc}) of 0.55 V, and a fill factor of 42.8, corresponding to an overall conversion efficiency of 0.88%. Under similar conditions, the photovoltaic parameters (J_{sc}, V_{oc}, and η) of cells with the FG_2 sensitizer are 13.35 mA cm^{-2}, 0.57 V, and 2.10%, respectively and shown in figure 47 below.

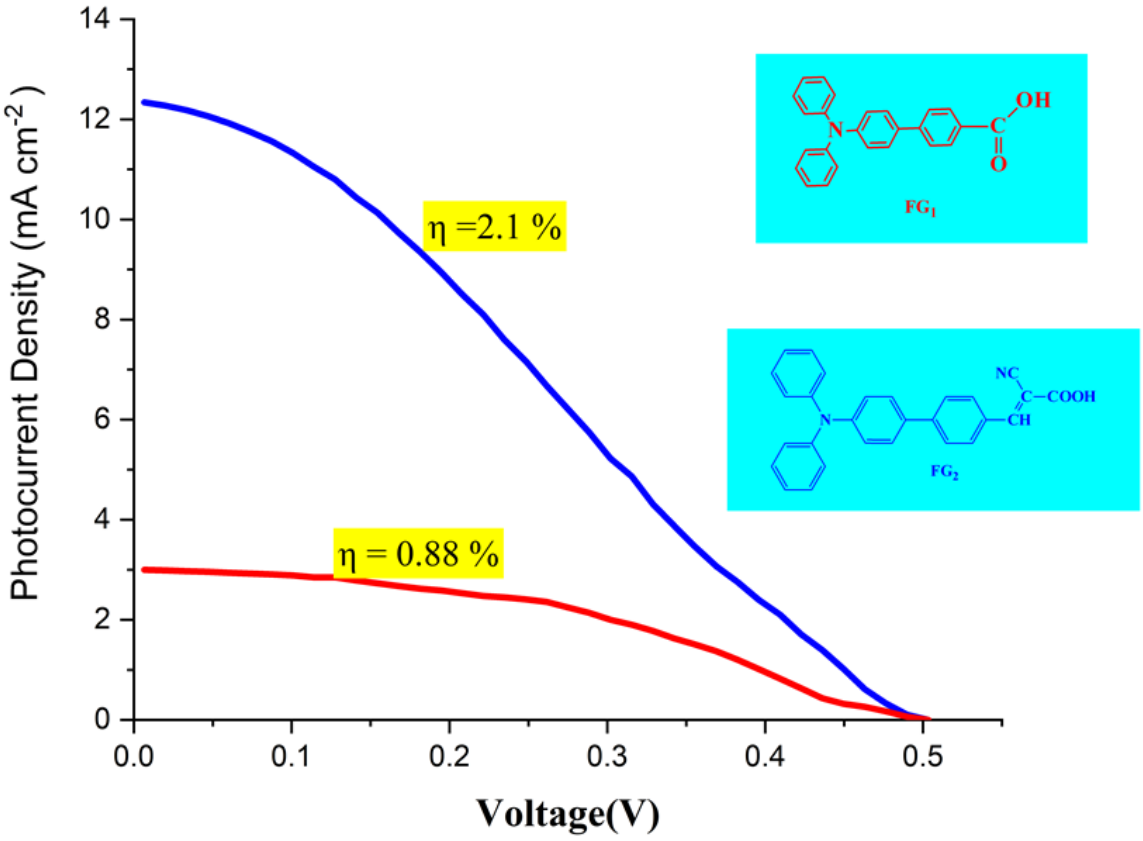

Figure 48 J-V curves of DSSCs sensitized with FG_1 and FG_2 dye under simulated AM1.5, 100 mW cm^{-2}.

The significant improvement of short circuit current density (J_{sc}) to FG_2 dye, due to better geometrical structure and also strongly bonded electro negative withdrawing group attached the anchoring unit which result the overall power conversion efficiency is high. The corresponding parameters short-circuit photocurrent density (J_{SC}), open-circuit photo voltage (V_{OC}), fill factor (ff), and power conversion efficiency (η) are listed in Table 1.

Table 1: shows the corresponding parameters short-circuit photocurrent density (J_{SC}), open-circuit photo voltage (V_{OC}), fill factor (ff), and power conversion efficiency (η).

Dye Source	V_{oc}	J_{sc} (mA/cm^{-2})	Fill factor (%)	η (%)
4'-(diphenylamino)-[1,1'-biphenyl]-4-carboxylic acid (FG_1)	0.55	3.75	42.81	0.88
(E)-2-cyano-3-(4'-(diphenylamino)-[1,1'-biphenyl]-4-yl) acrylic acid (FG_2)	0.57	13.35	27.04	2.10

4.4. Theoretical calculation

Using the Gaussian 09 W software program, the optimal structure and electron distribution of the two synthesized dye molecules were calculated using density functional theory (DFT) at the B3LYP functional and 6-31G ++ (d, p) basic set levels. According to the frontier MOs, HOMO (Highest Occupied Molecular Orbital) is the outermost orbital that contains electrons. It defines the ability to give electrons. In this study, electron-donating groups such as TPA increased the energy of the HOMO while decreasing the energy of the LUMO. The inner-most orbital containing free places that accept electrons are referred to as the LUMO (Lowest Unoccupied Molecular Orbital). It describes the ability to accept electrons.

In the ground state (HOMO) of the frontier MOs of 4'-(diphenyl amino)-[1,1'-biphenyl]-4-carboxylic acid (FG_1) dye, the electron distributed evenly on three phenyl rings of the TPA moiety and the same as also (E)-2-cyano-3-(4'-(diphenyl amino)-[1,1'-biphenyl]-4-yl) acrylic acid (FG_2) dye. On the other hand, FG_1 and FG_2 dye LUMO charge separation reside with carboxylic acid and cyanoacrylic acid anchoring unit group.

The energy gap of the dye is one of the key factors affecting the efficiency of the two dyes FG_1 and FG_2, a smaller value of energy band gap of FG_2 is highly desirable to maximize the efficiency of light harvesting by absorbing light at longer wave length in the Uv -Vis's spectra showed. The two synthetic FG_1 and FG_2 dyes the calculated energies and the energy gap is given by HOMO energy —LUMO energy as shown in Table 2.

Table 2: Band-gap Energies of calculation of the two-synthesis dye molecule calculated using B3LYP/6-31++G (d, p) basis sets.

Compound	**E_{HOMO} (eV)**	**E_{LUMO} (eV)**	**Energy gap $Eg_{(eV)}$**
4'-(diphenylamino)-[1,1'-biphenyl]-4-carboxylic acid (FG_1)	**-5.38**	**-2.04**	**3.34**
(E)-2-cyano-3-(4'-(diphenylamino)-[1,1'-biphenyl]-4-yl) acrylic acid (FG_2)	**-5.51**	**-2.89**	**2.62**

Both 4'-(diphenylamino)-[1,1'-biphenyl]-4-carboxylic acid (FG_1) and (E)-2-cyano-3-(4'-(diphenylamino)-[1,1'-biphenyl]-4-yl) acrylic acid (FG_2) dyes have anchoring groups are EWGs that reduce LUMO energy while having little effect on HOMO energy.

Table 3: Optimized geometries, distribution of HOMO-LUMO obtained from dyes FG_1 and FG_2 calculated at basis set of DFT, B3LYP/6-31G ++ (d, p).

Dye	HOMO	LUMO
FG_1	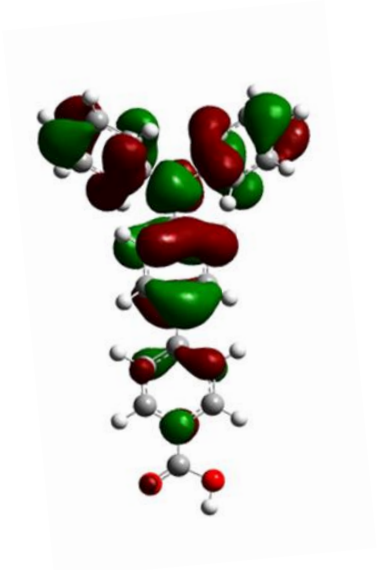	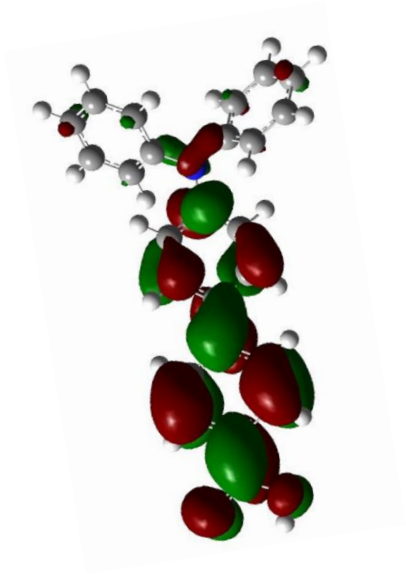
FG_2	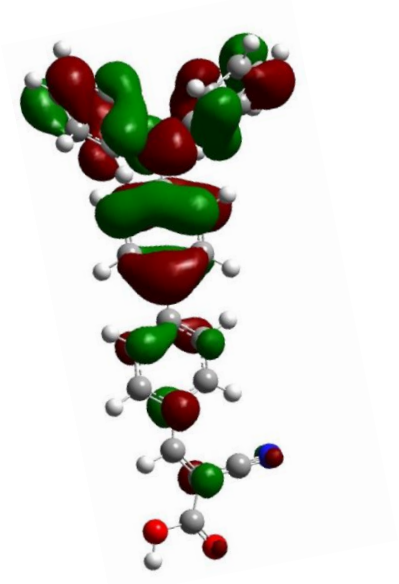	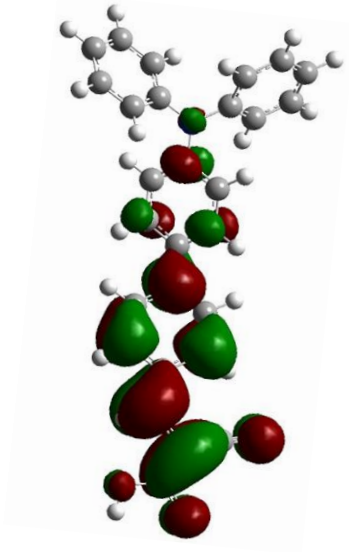

CHAPTER FIVE

5. CONCLUSION AND RECOMMENDATIONS

5.1. Conclusion

In conclusion, DSSCs could successfully synthesize, characterization, and fabrication two metal-free organic dyes based on TPA derivatives. Experimental and computational work that has shown that compounds FG_1 and FG_2 fulfill all the necessary conditions to operate as photosensitizers have allowed for an extensive study of the effect of efficiency utilizing derivatized metal-free organic dye. An analysis of the FT-IR and NMR spectra showed that the cyanoacetic acid anchoring mode on TiO_2 is responsible for the strong electro-withdrawing anchoring nature of FG_2 dye, which potentially causes increased efficiency. The device fabricated with the FG_2 sensitizer displayed the highest photon-to-current efficiency (PCE of 2.88 %). Its J_{SC} and V_{OC} were 14.13 mA cm^{-2} and 0.624 V, respectively. Further computational analyses of compounds FG_1 and FG_2 showed a significant electron density shift by the π-spacer from the triphenylamine donor to the acceptor/anchoring group.

5.2. Recommendations

The following issues are recommended for additional investigation: In this study, electron density was performed by applying the Gaussian 09 software using density functional theory. The photoanode materials of 4'-(diphenylamino)-[1,1'-biphenyl]-4-carboxylic acid (FG_1) and (E)-2-cyano-3-(4'-(diphenylamino)-[1,1'-biphenyl]-4-yl) acrylic acid (FG_2) and TPA-based symmetrical structures showed higher conversation energy for DSSCs. To prevent extremely high or low temperatures in future studies, the liquid electrolyte should be employed to assess the risk of evaporation. Moreover, combining the computational and experimental approaches to comprehend and investigate their molecular structure and assess the photoanode efficiency of TPA derivative molecular structures for DSSCs is preferable. However, the effects of extending molecular design by adding different donors and different acceptors on the building block of TPA derivative structure for low-cost DSSCs and other materials could be compared.

REFERANCE

A, M. Y., B, A. B., C, C. O., A, Z. S. ˇ, & Mika Sillanpa¨a. (2021). *Organic/metal-organic photosensitizers for dye-sensitized solar cells (DSSC): Recent developments, new trends, and future perceptions*. https://doi.org/https://doi.org/10.1016/j.dyepig.2021.109227

Ahmed, A., Mushtaq, I., & Chinnam, S. (2023). Suzuki–Miyaura cross-couplings for alkyl boron reagent: recent developments—a review. *Future Journal of Pharmaceutical Sciences*, *9*(1), 1–22. https://doi.org/10.1186/s43094-023-00520-1

Ahmed Azaid† a, Marzouk Raftani†a, Marwa AlaqarbehORCID logo*c, Rchid Kacimia, Tayeb AbramORCID logoa, Youness Khaddama, Diae Nebbacha, Abdelouahid Sbaia, T. L. and M. B. (2022). *New organic dye-sensitized solar cells based on the D–A–π–A structure for efficient DSSCs: DFT/TD-DFT investigations*. https://doi.org/DOI: 10.1039/D2RA05297K

Ajay Jain a, Richa Kothari b, V.V. Tyagi c, Reji Kumar Rajamony d e, Muhammad Shakeel Ahmad f, Har Mohan Singh g, Shubham Raina b, A. K. P. (2024). *Advances in organic solar cells: Materials, progress, challenges and amelioration for sustainable future*. https://doi.org/https://doi.org/10.1016/j.seta.2024.103632

Al-Alwani, M. A. M., Mohamad, A. B., Ludin, N. A., Kadhum, A. A. H., & Sopian, K. (2016). Dye-sensitised solar cells: Development, structure, operation principles, electron kinetics, characterisation, synthesis materials and natural photosensitisers. *Renewable and Sustainable Energy Reviews*, *65*, 183–213. https://doi.org/10.1016/j.rser.2016.06.045

Al-Shetwi, A. Q. (2022). *Sustainable development of renewable energy integrated power sector: Trends, environmental impacts, and recent challenges*. https://doi.org/https://doi.org/10.1016/j.scitotenv.2022.153645

Alfred Błaszczyk a, Katarzyna Joachimiak-Lechman b, Sylwia Sady a, Tomasz Tański c, Marek Szindler c, A. D. (2021). *Environmental performance of dye-sensitized solar cells based on natural dyes*. https://doi.org/https://doi.org/10.1016/j.solener.2020.12.040

Amineh, R. K. (2020). Applications of electromagnetic waves: Present and future.

Electronics (Switzerland), *9*(5), 15–18. https://doi.org/10.3390/electronics9050808

Ammar, hmed M., & , 1Hemdan S. H. Mohamed, 1, 2Moataz M. K. Yousef, 1Ghada M. Abdel-Hafez, 3Ahmed S. Hassanien, 1and Ahmed S. G. Khalil. (2019). *Dye-Sensitized Solar Cells (DSSCs) Based on Extracted Natural Dye*. https://doi.org/On this page Abstract Introduction Experimental Results and Discussion Conclusions Data Availability Conflicts of Interest Acknowledgments Supplementary Materials References Copyright Related Articles Research Article | Open https://doi.org/10.1155/2019/1867271

Ansari, A. A., Nazeeruddin, M. K., & Tavakoli, M. M. (2021). Organic-inorganic upconversion nanoparticles hybrid in dye-sensitized solar cells. *Coordination Chemistry Reviews*, *436*, 213805. https://doi.org/10.1016/j.ccr.2021.213805

Anshebo, G. A., Gebreyohanes, A. A., & Dessie, B. B. (2023). Green Energy: An Ideal Energy Solution for Sustainable Development of Afar Region, Ethiopia. *Journal of Energy*, *2023*, 1–11. https://doi.org/10.1155/2023/8849321

Asfaw, G. G., Benti, N. E., Desta, M. A., & Mekonnen, Y. S. (2023). *Design and fabrication of TiO2-based dye sensitized solar cells using plant-derived organic dyes*. https://doi.org/10.1063/5.0153639

Aslam, A., Mehmood, U., Arshad, M. H., Ishfaq, A., Zaheer, J., Ul Haq Khan, A., & Sufyan, M. (2020). Dye-sensitized solar cells (DSSCs) as a potential photovoltaic technology for the self-powered internet of things (IoTs) applications. *Solar Energy*, *207*(July), 874–892. https://doi.org/10.1016/j.solener.2020.07.029

Author links open overlay panelAnuj Tripathi, Vipin Kumar, P. C. (2022). *Impact of internal (donor/acceptor) moieties and π-spacer in triphenylamine-based dyes for DSSCs*. https://doi.org/https://doi.org/10.1016/j.jphotochem.2021.113738

Ayalew, M. E. (2022). DFT Studies on Molecular Structure, Thermodynamics Parameters, HOMO-LUMO and Spectral Analysis of Pharmaceuticals Compound Quinoline (Benzo[b]Pyridine). *Journal of Biophysical Chemistry*, *13*(03), 29–42. https://doi.org/10.4236/jbpc.2022.133003

Bayannavar, P. K., Mendhe, A. C., Sankapal, B. R., Sannaikar, M. S., Saba, S. K., Inamdar, S. R., & Kamble, R. R. (2021). Synthesis of metal free organic dyes: Experimental and theoretical approach to sensitize one-dimensional cadmium

sulphide nanowires for solar cell application. *Journal of Molecular Liquids*, *336*, 116862. https://doi.org/10.1016/j.molliq.2021.116862

Berry, M. J. (1991). ©19 9 1 Nature Publishing Group 그라첼꺼. *Nature*, *354*, 737–740.

Bist, A., & Chatterjee, S. (2021). *Review on Ef fi ciency Enhancement Using Natural Extract Mediated Dye-Sensitized Solar Cell for Sustainable Photovoltaics*. *2001058*, 1–19. https://doi.org/10.1002/ente.202001058

by Wadim Strielkowski 1, 2,*ORCID, L. C., Civín, L., Scholar, S. orgGoogl., & 2, Elena Tarkhanova 3ORCID, Manuela Tvaronavičienė 4, 5, O. andYelena P. 6ORCID. (2021). *Renewable Energy in the Sustainable Development of Electrical Power Sector: A Review*. https://doi.org/https://doi.org/10.3390/en14248240

Chaudhari, A. J., Kesarkar, V., Dhadve, N., Rao, B., Raut, S., & Patel, V. D. (2020). Experimental performance of glass based synthetic dye sensitized solar cell. *Materials Today: Proceedings*, *43*, 476–481. https://doi.org/10.1016/j.matpr.2020.12.019

Cheng Jih, C.-H. C. (2024). *Role of π-bridge and strong solid-state emission in triphenylamine-benzothiazole based nonlinear optical dyes*. https://doi.org/https://doi.org/10.1016/j.jphotochem.2023.115225

CO2 Emissions in 2022. (2023). *CO2 Emissions in 2022*. https://doi.org/10.1787/12ad1e1a-en

Conradie, J. (2024). *Effective dyes for DSSCs–Important experimental and calculated parameters*. https://doi.org/https://doi.org/10.1016/j.nexus.2024.100282

D’Alterio, M. C., Casals-Cruañas, È., Tzouras, N. V., Talarico, G., Nolan, S. P., & Poater, A. (2021). Mechanistic Aspects of the Palladium-Catalyzed Suzuki-Miyaura Cross-Coupling Reaction. *Chemistry - A European Journal*, *27*(54), 13481–13493. https://doi.org/10.1002/chem.202101880

Dominik Keiner, Ashish Gulagi, C. B. (2023). *Energy demand estimation using a pre-processing macro-economic modelling tool for 21st century transition analyses*. https://doi.org/https://doi.org/10.1016/j.energy.2023.127199

Driss FADILI a, Zakaria Mohyi Eddine FAHIM a, Abdelaaziz ALIOUI a, Si Mohamed BOUZZINE a b, M. H. a. (2024). *Enhancing optoelectronic properties of phosphonic acid based dyes via donor unit variation: A DFT/TD-DFT investigation*.

Editors@pv-magazine.com. (2024). *National Renewable Energy Laboratory (NREL)*.

Geldasa, F. T., Kebede, M. A., Shura, M. W., & Hone, F. G. (2023). Experimental and computational study of metal oxide nanoparticles for the photocatalytic degradation of organic pollutants: a review. *RSC Advances*, *13*(27), 18404–18442. https://doi.org/10.1039/d3ra01505j

Getachew Alemu, A., & Alemu, T. (2021). Solar Energy Potential and Future Prospects in Afar Region, Ethiopia. *American Journal of Modern Energy*, *7*(2), 22. https://doi.org/10.11648/j.ajme.20210702.12

Gielen, D., Boshell, F., Saygin, D., Bazilian, M. D., Wagner, N., & Gorini, R. (2019). The role of renewable energy in the global energy transformation. *Energy Strategy Reviews*, *24*(January), 38–50. https://doi.org/10.1016/j.esr.2019.01.006

Hailu, A. D., & Kumsa, D. K. (2020). Ethiopia renewable energy potentials and current state. *AIMS Energy*, *9*(1), 1–14. https://doi.org/10.3934/ENERGY.2021001

Han, L., Chen, Q., Yu, H., Lu, Y., & Jiang, S. (2021). Journal of Photochemistry & Photobiology , A : Chemistry Triphenylamine dyes bearing 4-phenyl-2- (thiophen-2-yl) thiazole bridge for dye sensitized solar cells. *Journal of Photochemistry & Photobiology, A: Chemistry*, *416*(May), 113341. https://doi.org/10.1016/j.jphotochem.2021.113341

Hira Kanwal 1 2, Ammar Ahmad Bilal Khan 1, Attaullah Shah 3, Muhammad Ubaidullah 1, Abbas Saeed Hakeem 5, Muhammad Younas 4, Tayyaba Ghani 1, M. M. (2024). *In-depth Investigation of Microstructure and Optical Properties of Tri-phase TiO2 Nanoparticles at Varied Calcination Temperatures for Dye Sensitized Solar Cells (DSSCs) Applications*. https://doi.org/Add to Mendeley Share Cite https://doi.org/10.1016/j.matchemphys.2024.129415

Hong Jiang, H.-Y. S. (2023). *Chapter 2 - Density-functional theory*. https://doi.org/https://doi.org/10.1016/B978-0-323-90049-2.00002-0

Ikpesu, J. E., Iyuke, S. E., Daramola, M., & Okewale, A. O. (2020). Synthesis of improved dye-sensitized solar cell for renewable energy power generation. *Solar Energy*, *206*(May), 918–934. https://doi.org/10.1016/j.solener.2020.05.002

Jean, J., Brown, P. R., Jaffe, R. L., Buonassisi, T., & Bulović, V. (2015). Pathways for solar photovoltaics. *Energy and Environmental Science*, *8*(4), 1200–1219.

https://doi.org/10.1039/c4ee04073b

Job, F., Mathew, S., Rajendran, R., Meyer, T., & Narbey, S. (2020). An investigation on the performance of dye-sensitized solar cell at various light intensities. *Materials Today: Proceedings*, *43*(xxxx), 3386–3390. https://doi.org/10.1016/j.matpr.2020.08.372

Kacimi, R., Raftani, M., Abram, T., Azaid, A., Ziyat, H., Bejjit, L., Bennani, M. N., & Bouachrine, M. (2021). Heliyon Theoretical design of D- π -A system new dyes candidate for DSSC application. *Heliyon*, *7*(May), e07171. https://doi.org/10.1016/j.heliyon.2021.e07171

Kamal Prajapat a 1, Mahesh Dhonde a 1, Kirti Sahu b, Prateek Bhojane c, VVS Murty d, P. M. S. (2023a). *The evolution of organic materials for efficient dye-sensitized solar cells*. https://doi.org/https://doi.org/10.1016/j.jphotochemrev.2023.100586

Kamal Prajapat a 1, Mahesh Dhonde a 1, Kirti Sahu b, Prateek Bhojane c, VVS Murty d, P. M. S. (2023b). *The semiconductor absorbs the electrons from the active dye and sends them to the external circuit to generate an electric current. Semiconductors provide a surface for dye binding. The crystallinity, morphology, and surface area of the semiconductor has* . https://doi.org/https://doi.org/10.1016/j.jphotochemrev.2023.100586

Karim, N. A., Mehmood, U., Zahid, H. F., & Asif, T. (2019). Nanostructured photoanode and counter electrode materials for efficient Dye-Sensitized Solar Cells (DSSCs). *Solar Energy*, *185*(March), 165–188. https://doi.org/10.1016/j.solener.2019.04.057

Kettle, J., Aghaei, M., Ahmad, S., Fairbrother, A., Irvine, S., Jacobsson, J. J., Kazim, S., Kazukauskas, V., Lamb, D., Lobato, K., Mousdis, G. A., Oreski, G., Reinders, A., Schmitz, J., Yilmaz, P., & Theelen, M. J. (2022). Review of technology specific degradation in crystalline silicon, cadmium telluride, copper indium gallium selenide, dye sensitised, organic and perovskite solar cells in photovoltaic modules: Understanding how reliability improvements in mature technolog. *Progress in Photovoltaics: Research and Applications*, *30*(12), 1365–1392. https://doi.org/10.1002/pip.3577

Khalida Abaid Samawi a, Ekhlas Abd-Alkuder Salman a, Belal Abd-Alsatar Alshekhly b, Maadh Fawzi Nassar c d, Mostafa Yousefzadeh Borzehandani c d, G. Abdulkareem-

Alsultan e, Muhammad Alif Mohammad Latif c f, E. A. c. (2022). *Rational design of different π-bridges and their theoretical impact on indolo[3,2,1-jk]carbazole based dye-sensitized solar cells*. https://doi.org/https://doi.org/10.1016/j.comptc.2022.113725

Lichun Sun, Dr. Yichuan Chen, Prof. Dr. Mengtao Sun, P. D. Y. Z. (2023). *Organic Solar Cells: Physical Principle and Recent Advances*. https://doi.org/https://doi.org/10.1002/asia.202300006

lR. Vinayagamoorthi a b, P. Balaji Bhargav a b, Nafis Ahmed a b, C. Balaji b, K. Aravinth a b, Akhil Krishnan a b, R. Govindaraj a b, P. R. a. (2023). *Recycling of end of life photovoltaic solar panels and recovery of valuable components: A comprehensive review and experimental validation*. https://doi.org/https://doi.org/10.1016/j.jece.2023.111715

Market, R. E. (2023). *Renewable power on course to shatter more records as countries around the world speed up deployment*.

Media, C. (2023). *Global renewables deployments to hit record levels in 2023*.

Mehran Farhang, Ali Reza Akbarzadeh, Mahboubeh Rabbani, A. M. G. (2022). *A retrospective-prospective review of Suzuki–Miyaura reaction: From cross-coupling reaction to pharmaceutical industry applications*. https://doi.org/https://doi.org/10.1016/j.poly.2022.116124

Mohamed Yahya a, Asmae Bouziani b, Cemil Ocak c, Zeynel Seferoğlu a, M. S. d. (2021). *Organic/metal-organic photosensitizers for dye-sensitized solar cells (DSSC): Recent developments, new trends, and future perceptions*. https://doi.org/https://doi.org/10.1016/j.dyepig.2021.109227

Navdeep Kaur, Samuel A. Oyon, Cheng-Yu Lai, D. R. R. (2023). *From reflection to absorption: Improving light harvesting of dye sensitized solar cells with Cu nanowires as reflectors*. https://doi.org/https://doi.org/10.1016/j.optmat.2023.114074

Obiora, S. C., Bamisile, O., Hu, Y., Ozsahin, D. U., & Adun, H. (2024). Assessing the decarbonization of electricity generation in major emitting countries by 2030 and 2050: Transition to a high share renewable energy mix. *Heliyon*, *10*(8), e28770. https://doi.org/10.1016/j.heliyon.2024.e28770

Phuti S. Ramaripa a, Kwena D. Modibane a b, Wilson M. Seleka a, Thabang R. Somo a, Edwin Makhado a, Katlego Makgopa c, T. B. O. (2024). *Recent applications of analytical techniques and electrochemical methods in characterizations of the titanium dioxide composites*. https://doi.org/https://doi.org/10.1016/j.ijoes.2023.100444

Popoola, M. D. & P. (2023). *Recent advances in solar photovoltaic materials and systems for energy storage applications: a review*. https://doi.org/https://doi.org/10.1186/s43088-023-00405-5

Prem Singh Saud a 1, Anup Bist a 1, Allison A. Kim b, Ayman Yousef c d, Ahmed Abutaleb c, Mira Park e f g, Soo-Jin Park h, B. P. (2024). *Dye-sensitized solar cells: Fundamentals, recent progress, and Optoelectrical properties improvement strategies*. https://doi.org/https://doi.org/10.1016/j.optmat.2024.115242

Prem Singh Saud a 1, Anup Bist a 1, Allison A. Kim b, Ayman Yousef c d, Ahmed Abutaleb c, Mira Park e f g, Soo-Jin Park h, B. P. e. (2024). *Dye-sensitized solar cells: Fundamentals, recent progress, and Optoelectrical properties improvement strategies*. https://doi.org/https://doi.org/10.1016/j.optmat.2024.115242

Rabaia, M. K. H., Abdelkareem, M. A., Sayed, E. T., Elsaid, K., Chae, K. J., Wilberforce, T., & Olabi, A. G. (2021). Environmental impacts of solar energy systems: A review. *Science of the Total Environment*, *754*, 141989. https://doi.org/10.1016/j.scitotenv.2020.141989

Ramanujam, J., Bishop, D. M., Todorov, T. K., Gunawan, O., Rath, J., Nekovei, R., Artegiani, E., & Romeo, A. (2020). Flexible CIGS, CdTe and a-Si:H based thin film solar cells: A review. *Progress in Materials Science*, *110*, 100619. https://doi.org/10.1016/j.pmatsci.2019.100619

Sharma, G., Singh, V., Dolia, S. N., Jain, I. P., Jain, P. K., & Lal, C. (2023). Present status of metal-free photosensitizers for dye-sensitized solar cells. *Materials Today: Proceedings*, *February*. https://doi.org/10.1016/j.matpr.2023.02.179

Sharma, K., Sharma, V., & Sharma, S. S. (2018). Dye-Sensitized Solar Cells: Fundamentals and Current Status. *Nanoscale Research Letters*, *13*. https://doi.org/10.1186/s11671-018-2760-6

Statista. (2024). *Global CO2 emissions by year 1940-2023*.

Subhasri Kar a, Sumit Banerjee b, C. K. C. (2023). *Performance study of Amorphous-Si thin-film solar cell for the recent application in photovoltaics*. https://doi.org/Add to Mendeley Share Cite https://doi.org/10.1016/j.matpr.2023.01.058

Suzaimi Johari, a M. R. J. and N. G. K. (2022). *An overview of metal-free sustainable nitrogen-based catalytic knoevenagel condensation reaction*. https://doi.org/DOI https://doi.org/10.1039/D2OB00135G

Taylor, C. N. (2021). *Hydrogen and its detection in fusion and fission nuclear materials – a review*. https://doi.org/https://doi.org/10.1016/j.jnucmat.2021.153396

Węgierek, J. P. and P. (2022). *Photovoltaic Cell Generations and Current Research Directions for Their Development*. https://doi.org/doi: 10.3390/ma15165542

Weldemicheal, H. T., Desta, M. A., & Mekonnen, Y. S. (2023). Derivatized photosensitizer for an improved performance of the dye-sensitized solar cell. *Results in Chemistry*, *5*(October 2022), 100838. https://doi.org/10.1016/j.rechem.2023.100838

Wilk, M., Trzepizur, D., Koszelewski, D., Brodzka, A., & Ostaszewski, R. (2019). Synthesis of (E)-α,β-unsaturated carboxylic esters derivatives from cyanoacetic acid via promiscuous enzyme-promoted cascade esterification/Knoevenagel reaction. *Bioorganic Chemistry*, *93*(January). https://doi.org/10.1016/j.bioorg.2019.02.041

Yahya, M., Bouziani, A., Ocak, C., Seferoğlu, Z., & Sillanpää, M. (2021). Organic/metal-organic photosensitizers for dye-sensitized solar cells (DSSC): Recent developments, new trends, and future perceptions. *Dyes and Pigments*, *192*(January). https://doi.org/10.1016/j.dyepig.2021.109227

Zani, L., Dessì, A., Franchi, D., Calamante, M., Reginato, G., & Mordini, A. (2019). Transition metal-catalyzed cross-coupling methodologies for the engineering of small molecules with applications in organic electronics and photovoltaics. *Coordination Chemistry Reviews*, *392*, 177–236. https://doi.org/10.1016/j.ccr.2019.04.007

Zhang, B., & Sun, L. (2019). Artificial photosynthesis: Opportunities and challenges of molecular catalysts. *Chemical Society Reviews*, *48*(7), 2216–2264. https://doi.org/10.1039/c8cs00897c

Zhang, T., Wang, M., & Yang, H. (2018). A review of the energy performance and life-

cycle assessment of building-integrated photovoltaic (BIPV) systems. *Energies*, *11*(11). https://doi.org/10.3390/en11113157